A novel role of PRL in regulating epithelial cell density by inducing apoptosis at confluence

Doctoral Thesis

Sweksha Lohani

Department of Cellular Regulation,
Research Institute for Microbial Diseases (RIMD),
Graduate School of Frontier Biosciences,
Osaka University
March, 2021

Summary

Maintaining proper epithelial cell density is essential for the survival of multicellular organisms. While regulation of cell density through apoptosis is well known, its mechanistic details remain elusive. Here, I report the involvement of membrane-anchored phosphatase of regenerating liver (PRL), originally known for its role in cancer malignancy, in this process. In epithelial MDCK cells, upon confluence, doxycycline-induced expression of PRL upregulated apoptosis, reducing the cell density. This could be circumvented by artificially reducing the cell density via stretching the cell-seeded silicon chamber. Moreover, siRNA-mediated knockdown of endogenous PRL blocked apoptosis, leading to greater cell density. Mechanistically, PRL promoted apoptosis by upregulating the translation of E-cadherin and activating TGF-β pathway. Morpholino-mediated inhibition of PRL expression in zebrafish embryos caused developmental defect with reduced apoptosis and increased epithelial cell density during convergent extension. This study revealed a novel role of PRL in regulating density-dependent apoptosis in vertebrate epithelium.

Table of Contents

List of abbreviations

ALK5 : anaplastic lymphoma kinase 5

AP : alkaline phosphatase

BrdU : 5-Bromo-2´-deoxy-uridine

CBB : coomassie brilliant blue

CBS : cystathionine β-synthase

CHX : cycloheximide

CNNM : cyclin M

CUGBP1 : CUG-binding protein 1

DAPI : 4´,6-diamidino-2-phenylindole

DMEM : Dulbecco's modified Eagle's medium

DMSO : dimethylsulphoxide

Dox : doxycycline

DSP : dual specificity phosphatase

DUF : domain of unknown function

eIF : eukaryotic translation initiation factor

FBS : fetal bovine serum

FPKMs : fragments per kilobase of exon per million mapped reads

FZR1 : fizzy and cell division cycle 20 related 1

hpf : hour post-fertilization

HuR : Human antigen R

KO : knockout

LATS : large tumor suppressor

LDH : lactate dehydrogenase

MAP4K : mitogen-activated protein kinase kinase kinase kinase

MDCK : Madin-Darby Canine Kidney

MET : mesenchymal-to-epithelial transition

MO : morpholino oligonucleotide

MST : mammalian Ste20-like kinase

mTOR : mammalian target-of-rapamycin

N.S. : not-significant

PABP : poly(A)-binding protein

PBS : phosphate-buffered saline

PDMS : polydimethylsiloxane

PFA : paraformaldehyde

PRL : phosphatase of regenerating liver

PTEN : phosphatase and tensin homolog

PTP : protein tyrosine phosphatase

qPCR : quantitative PCR

RBP : RNA-binding protein

RT : room temperature

S1P : sphingosine-1 phosphate

$S1P_2$: sphingosine-1 phosphate receptor 2

TEER : transepithelial electrical resistance

UTR : untranslated region

YAP : Yes-associated protein

ZO-1 : zonula occludens-1

General Introduction

This study details the importance of oncogenic phosphatase of regenerating liver (PRL) in the regulation of epithelial cell density in the vertebrate epithelium. The following facts about PRL have been reported by now.

Phosphatase of regenerating liver (PRL)

PRL is a membrane anchoring molecule of approximately 20 kDa and its gene is conserved in every eukaryotic kingdom (Hardy et al., 2018). In mammals, PRL family constitutes of three family members: PRL1, PRL2, and PRL3. Originally, PRL1 was discovered as strongly upregulated immediate-early gene product in regenerating liver after partial hepatectomy (Diamond et al., 1994). Later, other two PRLs (PRL2 and PRL3) were identified by searching database for sequence homologous to PRL1 (Zeng et al., 1998). The amino-acid sequence of PRL2 is 87% identical to PRL1, while that of PRL3 is 76% and 79% identical to PRL1 and PRL2, respectively (Bessette et al., 2008). It has been reported that the secondary structure as well as overall protein folding is highly similar among PRLs (Bessette et al., 2008). From the structure and site-directed mutagenesis experiments, unlike classical tyrosine phosphatase, PRL is categorized as a dual specificity phosphatases (DSPs), although the sequence identity with typical DSPs is lower than 30% (Kozlov et al., 2004; Bessette et al., 2008). In general, DSPs have ability to dephosphorylate both tyrosine and serine/threonine residues, and are known to act on diverse substrates to mediate wide variety of cellular response (Tonks, 2006).

Structural features

PRL is a small phosphatase molecule that consist of single catalytic protein tyrosine phosphatase (PTP) domain on its N-terminal end (Figure 1). One of the unique features of PRL among all the other phosphatases is the presence of prenylation domain on its C-terminal end. The prenylation motif has been reported to play an important role in the membrane anchorage, since ectopic expression of PRL containing mutation within the prenylation sequence diminishes its membrane localization and results in the diffused pattern of expression within the cytoplasm (Zeng et al., 2000; Sun et al., 2005).

Phosphatase activity and cyclin M (CNNM)-binding ability

PRL has been reported to show phosphatase activity towards certain substrates such as ezrin, phosphatidylinositol (4,5) bisphosphate, integrin β1, fizzy and cell division cycle 20 related 1 (FZR1), and phosphatase and tensin homolog (PTEN) (Forte et al., 2008; McParland et al., 2011; Tian et al., 2012; Zhang et al., 2019; Li et al., 2020). The cysteine residue, Cys104, within the catalytic domain is conserved among all three members of PRL family, and is indispensable for the regulation of phosphatase activity (Yu et al., 2007). Like other PTPs, the catalytic cysteine residue of PRL forms a thiophosphoryl enzyme intermediate during the dephosphorylating process, and the aspartate residue within the catalytic domain then facilitates the hydrolysis of enzyme-phosphate complex, thereby releasing the phosphate group and making the enzyme ready for the next phosphatase reaction (Wei et al, 2018). However, the analyses of enzymatic activity of PRL using its artificial substrates demonstrated that the phosphatase activity of PRL is extremely low compared to other typical tyrosine phosphatases (Kozlov et al, 2004). One of the possible reasons is the presence of alanine residue (Ala111) within the catalytic

domain, which is occupied by serine or threonine residue in most PTPs (Sun et al, 2005). The serine or threonine residue has been believed to play an important role in the hydrolysis of enzyme-phosphate complex in most PTPs (Sun et al, 2005). Therefore, replacement of serine or threonine with alanine in PRL might have increased the half-life of thiophosphoryl enzyme intermediate. This was supported by an experiment using PRL1 mutant that replaces alanine with serine (A111S), where the upregulation of catalytic activity of PRL towards its synthetic substrate was observed (Sun et al, 2005). Except for the phosphatase activity, PRL interacts with a Mg^{2+} transporter CNNM (Figure 2) (Funato et al., 2014; Hardy et al., 2015; Gulerez et al., 2016). CNNM constitutes a family of four members (CNNM1 to CNNM4) and involved in the efflux of Mg^{2+} from the cell by exchanging it with Na^{+} (Funato et al., 2014). CNNM has two evolutionarily conserved domains: membrane-spanning domain of unknown function (DUF) 21 domain, and intracellular cystathionine β-synthase (CBS) domain (de Baaij et al., 2012). PRL has been reported to interact with the CBS domain of CNNM and inhibits the ion transport (Funato et al., 2014; Hardy et al., 2015). The co-immunoprecipitation experiment easily detected endogenous PRL-CNNM complex, suggesting the presence of strong interaction between these two molecules (Funato et al., 2014).

Tissue Expression

PRL2 is the most abundantly expressed family member of PRL in human tissues which shows ubiquitous expression (Dumaual et al., 2006). Similarly, PRL1 also shows widespread distribution, but its expression level is lower compared to PRL2. On the other hand, PRL3 is primarily expressed in heart and skeletal muscle, although low level of its expression is detectable in number of other tissues (Zeng et al., 1998; Matter et al., 2001).

The ubiquitous expression of PRLs in different tissues suggest that they might be essential for the basic cellular processes.

Role of PRL in cancer progression

PRL gained much attention since 2001, when Vogelstein's research group reported *PRL3* as the highly overexpressed gene in the metastases of all the colorectal cancers they have examined (Saha et al., 2001). Later, extensive studies of PRL in relation with malignant progression of several types of cancers such as breast cancer, colorectal cancer, gastric cancers have been reported (Bessette et al., 2008). The upregulation of PRL expression often correlates with poor patient prognosis (Bessette et al., 2008), however the detailed mechanism of how PRL plays a role in the malignant progression of cancer remains elusive. Some studies suggest that phosphatase activity of PRL is important for the cancer malignancy (Guo et al., 2004), while recent studies have reported that phosphatase activity is dispensable but its interaction with CNNM is rather essential (Funato et al., 2014; Kozlov et al., 2020). Importantly, the increased expression of PRL is often observed at advanced stages compared to early stages of cancer (Saha et al., 2001; Polato et al., 2005; Radke et al., 2006; Dai et al., 2009; Mayinuer et al., 2013). Therefore, it is likely that cancer malignancy promoting role of PRL is critical at relatively late stage of cancer.

Tumor suppressive role of PRL

Contrary to cancer malignancy promoting role of PRL, some studies have reported the tumor suppressive role of PRL. Basak et al. reported *Prl3* as a p53-inducible gene, where the overexpression of Prl3 downstream of p53, results in G_1 arrest of cell cycle (Basak et al., 2008). Furthermore, they have suggested that basal Prl3 level is essential for the

normal progression of cell cycle, as the knockdown of Prl3 expression also triggers the arrest response. Besides, in *Drosophila melanogaster*, overexpression of PRL1, a sole ortholog of PRL, significantly suppresses the Src-induced oncogenic effect such as massive growth and developmental disorganization in the developing wing (Pagarigan et al., 2013). Therefore, these findings suggest that in the context of non-transformed cells, PRL seems to possess roles other than progression of cancer malignancy.

Physiological role of PRL

The physiological role of PRL remains poorly understood. To reveal this, PRL knockout (KO) mice have been generated, but *Prl1*-KO or *Prl3*-KO mice showed no observable phenotypic alterations and *Prl2*-KO mice showed only mild phenotypes such as growth retardation and reduced fertility (Figure 3) (Bai et al., 2016; Dong et al., 2012; Dong et al., 2014; Zimmerman et al., 2013). Importantly, double KO for *Prl1* and *Prl2*, the two highly expressed PRL family members, were found to be embryonic lethal (Figure 3) (Bai et al., 2016). Bai et al. further investigated at which stage the embryos were dead by harvesting embryos at different stages. Unfortunately, no embryos were found viable at embryonic day 9.5 (E9.5), the earliest stage they have examined (Bai et al., 2016). Therefore, PRLs seem to possess a critical function during early embryonic development, but the functional details remain largely unknown. In addition, as either *Prl1*-KO or *Prl2*-KO mice were viable, but double KO for *Prl1* and *Prl2* were embryonic lethal, there seems to be functional redundancy between PRLs. In *Drosophila melanogaster*, the KO of Prl1, the only one mammalian homolog of PRL, resulted in irreversible wing hold up phenotype, while the overexpression of Prl1 particularly in the nervous system rescued this mutant phenotype (Guo et al., 2019). From further experiments, authors have found

that Prl1 has neuroprotective role. Besides, the knockout of PRL3 in zebrafish suppressed the melanocyte stem cell differentiation and found to prevent premature melanoblast expansion (Johansson et al., 2020). Except for these, large part of function of PRL remains elusive.

Introduction

Epithelial cells are tightly connected to each other through cell-cell junctions and form a sheet-like structure. The cell density of an epithelial sheet is exquisitely homeostatic, which is essential for its coordinated function in shaping and maintaining the body of multicellular organisms. One of the classical mechanisms that maintain optimum cell density is contact inhibition of proliferation or, in short, contact inhibition, whereby cells stop dividing, when they come in contact with each other at confluence (Abercrombie and Heaysman, 1954; Eagle and Levine, 1967). Mechanism of contact inhibition has been extensively studied, and the implication of various molecules affecting diverse cellular functions, such as cell adhesion, polarization, and proliferation, has been reported (McClatchey and Yap, 2012). In particular, the importance of Hippo signaling is recognized in transmitting the information of cell-cell contact to the nucleus, which is crucial for contact inhibition. In brief, mechanical cues arising from cell adhesion and the cytoskeleton can mediate the downstream activation of large tumor suppressor (LATS), directly or indirectly through mammalian Ste20-like kinase (MST) or mitogen-activated protein kinase kinase kinase kinase (MAP4K) (Ma et al., 2019). Activated LATS then phosphorylates the transcriptional coactivator Yes-associated protein (YAP), and prevents its nuclear translocation, and the subsequent transcriptional activation of growth-promoting target genes (Zhao et al., 2007; Zhao et al., 2008). Alternative mechanisms of maintaining optimal cell density, through extruding the apoptotic or live-cells from the epithelial sheet, have also been demonstrated. Apoptotic cell extrusion was originally reported in chick embryonic epithelium and in the cultures of Madin-Darby Canine

Kidney (MDCK) cells, which show typical characteristics of epithelial cells (Rosenblatt et al., 2001), while overcrowding-induced live cell extrusion was first identified in the epithelium of *Drosophila melanogaster* and MDCK cell cultures (Marinari et al., 2012; Eisenhoffer et al., 2012). In both cases, the extrusion of cells is preceded by the production of sphingosine-1 phosphate (S1P), which then activates S1P receptor 2 ($S1P_2$) on the neighboring cells, and induces ROCK-dependent actomyosin contraction, to expel cells from the epithelial sheet (Gu et al., 2011; Eisenhoffer et al., 2012). Furthermore, at high cell density, the activation of Piezo-1, a stretch-activated calcium channel, triggers the overcrowding-induced live cell extrusion (Eisenhoffer et al., 2012). On the other hand, what drives cell death and how it is regulated in apoptotic cell extrusion are not understood well.

PRL is a family of prenylated proteins anchored to the plasma membrane, and has three members (PRL1, PRL2 and PRL3) in mammals (Diamond et al., 1994; Zeng et al., 1998). In 2001, Saha et al. reported *PRL3* as a highly overexpressed gene in the metastases of all colorectal cancers examined (Saha et al., 2001), and later, a number of studies have reported a link between overexpression of PRL and malignant progression of several types of cancers (Bessette et al., 2008). Several studies using cultured cancer cells showed that PRL overexpression can promote cell proliferation, migration, and invasion (Bessette et al., 2008), suggesting its role in promoting cancer progression. On the other hand, some studies have reported tumor-suppressive actions of PRL. *Prl3* is a direct target gene of p53 tumor suppressor in primary mouse fibroblasts, and its overexpression negatively regulates the cell cycle progression (Basak et al., 2008). In *Drosophila melanogaster*, overexpression of PRL1, a sole PRL ortholog, counteracts the oncogenic effect of Src (Pagarigan et al., 2013). These observations suggest that, in non-

transformed cells, PRL probably has a function other than promoting cancer malignancy. To examine the normal physiological functions of PRL, gene knockout (KO) mice have been generated. *Prl1*-KO and *Prl3*-KO mice developed normally and showed no obvious phenotypic alterations (Bai et al., 2016; Zimmerman et al., 2013), while *Prl2*-KO mice showed mild changes in the phenotype, such as growth retardation and reduced fertility (Dong et al., 2012; Dong et al., 2014). Double KO mice for *Prl1* and *Prl2* were embryonic lethal (Bai et al., 2016). These observations suggest that PRLs are essential for normal embryonic development, but the functional details are not clear. In the previous study, MDCK epithelial cells with doxycycline (Dox)-inducible PRL-expression was established, which showed unique properties, when stimulated with growth factors or under acidic condition (Kojima et al., 2019; Funato et al., 2020). However, under normal culture conditions, PRL expression did not affect the basic properties of cells, such as proliferation rate, overall morphology, and cell-cell adhesion. As is often the case with *in vitro* culture experiments, cells were seeded and cultured relatively sparsely in these studies. Therefore, in the present study, I performed detailed analyses of cells after they reached confluence. From a series of experiments, I found that PRL regulates the cell density in epithelial sheets by promoting apoptosis, mediated by the translational elevation of E-cadherin expression and downstream activation of TGF-β pathway. Moreover, using zebrafish, I found that PRL plays a critical role in the control of epithelial cell density during convergent extension, a critical process in the early development of vertebrate embryos.

Results

Expression of PRL suppresses dome formation at confluence

To examine the effect of the expression of PRL in epithelial cells, I used two independent MDCK cell lines that can express GFP-tagged PRL3 (PRL #1 and PRL #2), when induced with Dox (Kojima et al., 2019). I cultured the cells after they reached confluence and observed the changes in the morphological characteristics. As shown in Figure 4A, culture of the control cells showed sporadic formation of round and swollen structures, which was completely suppressed upon PRL expression. Similar results were observed when the double the number of cells were seeded (Figure 4B). Formation of such swollen structures were also observed when the cells were cultured without Dox, thereby confirming the effect of PRL expression (Figure 4A). I tested the effects of expressing C104S, a mutant PRL3 that lacks both phosphatase activity and Mg^{2+} transporter CNNM-inhibiting activity, which made it functionally inactive in promoting tumor development (Guo et al., 2004; Kozlov et al., 2004; Funato et al., 2014). The results showed the formation of swollen structures as in control cells, suggesting the importance of functional PRL in this process (Figure 4A). Furthermore, I investigated the sheet structure in detail by staining filamentous actin with phalloidin and constructed three-dimensional images through confocal microscopy. The interior of the swollen structure was empty, as shown in the images of horizontal sections (Figure 4C). Vertical sections, reconstructed by stacking the images of the horizontal sections, showed that each cell sheet was single-layered, but some regions in the cultured sheets were found to be detached from the surface of glass coverslips. From these observations, I confirmed that the round and

swollen structures observed were ‘domes’ containing a fluid-filled internal space, as described earlier (Leighton et al., 1969).

Domes are formed in the confluent culture of MDCK cells due to the transport of salt and water across the epithelial monolayer, which accumulate between the epithelial sheet and culture dish (Cereijido et al., 1981). As the creation of a dome requires the formation of a functional epithelial barrier, establishment of apicobasal polarity, and high cell density in the culture (Misfeldt et al., 1976; Cereijido et al., 1980), next I examined whether these requirements were met in the PRL-expressing cells. First, I evaluated the functional epithelial barrier by measuring transepithelial electrical resistance (TEER), a widely accepted quantitative parameter to measure the integrity of tight junctions, across the epithelial sheet (Srinivasan et al., 2015). The TEER value of the control cells was 83.6 ± 4.1 Ωcm^2, and that of PRL-expressing cells was 317.9 ± 14.8 Ωcm^2 (mean ± SD), which established the high TEER of PRL-expressing cells, and suggested the presence of a functional epithelial barrier. Next, to test the integrity of apicobasal polarity, I performed immunostaining for tight junction marker zonula occludens-1 (ZO-1) (Stevenson et al., 1986), adherens junction markers E-cadherin (Takeichi, 1977) and β-catenin (McCrea et al., 1991), and basolateral marker Na^+/K^+ ATPase (Skou, 1957) (Figure S1), and found no alteration in the expression pattern of any of them. This suggested that the establishment of polarized epithelium was not affected by the status of PRL expression. Therefore, I focused on the cell density of each culture in greater details.

PRL expression lowers the cell density of epithelial cell-sheet

I stained the nuclei in each cultured cell-sheet, to determine the cell density. I found that PRL expression led to lower cell density, whereas the expression of C104S mutant was

ineffective in this regard (Figure 5A). These results suggest the importance of PRL in lowering the cell density of epithelial sheets. By changing the number of cells used for seeding, I found that each cell culture has its own upper limit of epithelial cell density (Figure 5B). Notably, the maximum cell density was significantly decreased with induction of PRL expression. When I compared the proliferation status of cells at 24 h and 48 h after Dox treatment, I found no significant difference in the percentage of proliferating cells (Figure S2A and S2B). Next I examined through cytotoxicity assay whether PRL expression promoted cell death. The results showed that when the cells were seeded at high density, PRL expression enhanced the release of lactate dehydrogenase (LDH), a cytosolic enzyme, from the damaged cells (Figure 5C). Interestingly, the LDH release in the PRL-expressing cells was critically dependent on cell density, as it decreased significantly at lower cell density. I then determined the extent of apoptosis by immunostaining with cleaved caspase-3. Again, expression of PRL at high cell density greatly stimulated apoptotic cell death (Figure 5D and 5F), while it was suppressed at low cell density (Figure 5E and 5F), thus proving the density-dependent induction of apoptosis by PRL. To corroborate this finding, I seeded cells in a silicon chamber, and stretched the chamber to artificially reduce the epithelial cell density (Figure 5G). Apoptosis was drastically suppressed when epithelial cell density was lowered by stretching the chamber (Figure 5H and 5I), thereby demonstrating the importance of cell density in PRL-induced apoptosis.

Next, to confirm the importance of endogenous PRL in the density-dependent cell death, I knocked down endogenous PRL1 and PRL2, the two most abundant PRL isoforms expressed in MDCK cells, with siRNA (Kojima et al., 2019). For this, I analyzed the cells fixed at 48 h after Dox treatment, when the rate of apoptosis is significantly

higher in control cells. Transfection with two different siRNAs for *PRL1* or *PRL2* significantly reduced PRL1 or PRL2, respectively (Figure 6A). In fact, knocking down either PRL1 or PRL2 reduced apoptosis significantly (Figure 6B and 6C), and increased the cell density concomitantly (Figure 6B and 6D). It should be noted that the effect of knocking down PRL2, which is expressed more than PRL1 in MDCK cells (Figure 6A), was more drastic. However, double knockdown of PRL1 and PRL2 seemed to damage the cells, and they became sparse (Figure S3), hindering further analyses. Overall, I concluded that endogenous PRL also regulates epithelial cell density, probably through induction of apoptosis.

Increased expression of E-cadherin is necessary for driving cell death

As shown in Figure S1, immunostaining of PRL-expressing cells with anti-E-cadherin antibodies showed a brighter staining signal. As expected, immunoblotting with anti-E-cadherin antibodies showed a significant increase in E-cadherin expression (Figure 7A). Several studies have reported that increased expression of E-cadherin induces cell death (Lu et al., 2014; Akieda et al., 2019). I determined the effect of E-cadherin knockdown on the density-dependent cell death. As shown in Figure 7B, transfection with *E-cadherin* siRNA targeting two different sequences, suppressed the E-cadherin expression. Immunostaining with anti-cleaved caspase-3 antibody showed a significant suppression of apoptosis in PRL-expressing cells (Figure 7C and 7D).

To understand how PRL increases the E-cadherin expression, first I measured the levels of *E-cadherin* mRNA by quantitative PCR, but found no significant increase in PRL-expressing cells (Figure S4A). Stability of the E-cadherin protein was also not increased by PRL expression (Figure S4B and S4C). Therefore, I speculated that probably

the translation of *E-cadherin* mRNA was enhanced in PRL-expressing cells. Autoradiography of total proteins, with 30 min radiolabeling using [^{35}S]methionine and [^{35}S]cysteine, showed comparable labeling in control and the PRL-expressing cells (Figure 7E), suggesting no significant difference in global protein synthesis. Immunoprecipitation of each radiolabeled lysate with anti-E-cadherin antibodies (Figure 7F), showed a five-fold increase in the newly synthesized E-cadherin in PRL-expressing cells (Figure 7G), indicating a significant enhancement of E-cadherin translation in PRL-expressing cells.

TGF-β pathway drives cell death downstream of E-cadherin

Next I sought to understand what drives apoptosis downstream of E-cadherin. Several studies have reported E-cadherin-dependent activation of TGF-β pathway (Andl et al., 2006; Akieda et al., 2019), which in turn, triggers cell death downstream of them. In the canonical TGF-β pathway, ligand binding stimulates the TGF-β receptor type II to complex with the type I receptor (also known as anaplastic lymphoma kinase 5: ALK5), which allows the type II receptor to phosphorylate the kinase domain of ALK5. Activated ALK5 propagates the signal further by phosphorylating the receptor-regulated effector proteins (R-Smads, consisting of Smad2 and Smad3). Phosphorylated R-Smads then recruit co-Smad (Smad4) to form a trimolecular complex, which translocates into the nucleus, and stimulates the transcription of the target genes (Shi and Massagué, 2003). To examine the activation status of TGF-β pathway in PRL-expressing cells, I investigated the localization of Smad2 by immunostaining. I found an approximately two-fold increase in the nuclear to cytoplasmic Smad2 signal ratio, which is comparable to the levels after TGF-β stimulation (Figure 8A and 8B). Importance of E-cadherin in

nuclear translocation of Smad2 was confirmed by siRNA-mediated knockdown of *E-cadherin*, which resulted in a partial, but significant reduction in the signal ratio (Figure 8C and 8D). When ALK5 was inhibited in PRL-expressing cells using two chemical inhibitors, viz., ALK5 inhibitor II and SB525334, both of which are known to suppress TGF-β signaling (Ichida et al., 2009; Laping et al., 2007), apoptosis was partially, but significantly reduced (Figure 8E and 8F), suggesting the involvement of ALK5 in induction of apoptosis in PRL-expressing cells. In addition, siRNA-mediated knockdown of Smad4, a component essential for the activation of TGF-β signaling (Liu et al., 1997), had similar effects (Figure 8G-8I). Overall, I found that activation of TGF-β pathway downstream of E-cadherin contributes to drive apoptosis in PRL-expressing cells.

PRL regulates epithelial cell density and convergent extension in zebrafish embryos

To examine the *in vivo* role of PRL in controlling epithelial cell density, I studied its effects on the embryonic development of zebrafish, in which changes in the epithelial cell density can be observed. Firstly, I overexpressed PRL3 in zebrafish embryos by injecting mouse *Prl3* mRNA, and observed for the phenotype. However, preliminary result showed several phenotypes that can arise from different causes (Appendix 1A and 1B), possibly due to overexpression of mouse Prl, and overexpression in unusual tissues where the endogenous level of PRL is low. As it was difficult to narrow down the developmental stages at which PRL has a critical role, I decided to suppress the endogenous PRL in zebrafish embryos. Zebrafish has five isoforms of PRL genes: *ptp4a1*, *ptp4a2a*, *ptp4a2b*, *ptp4a3a*, and *ptp4a3b*. As RNA sequencing showed that the expression levels of *ptp4a3a* and *ptp4a3b* were remarkably low at the shield-stage, 6 h post-fertilization (hpf) and at tail-bud-stage, 10 hpf (Figure 9A), I decided to suppress the expression of the remaining

three isoforms, *ptp4a1*, *ptp4a2a*, and *ptp4a2b*, with translation-blocking anti-sense morpholino oligonucleotides (MOs). As there are two splicing variants for *ptp4a2b*, *variant 1* and *variant 2*, MOs specifically targeting each of them were designed. To verify the effectiveness of each MO, four *EGFP*-fused mRNA constructs, containing MO target sites for the above genes, were synthesized (Figure S5A). Co-injection of each MO with the respective *EGFP*-fused mRNA construct resulted in almost complete suppression of GFP signal (Figure S5B), confirming the suppression of mRNA translation. When each of the MO was injected into one-cell-stage zebrafish embryos, those injected with *ptp4a2b variant 1* MO showed mild shortening of the anterior-posterior axis at 24 hpf (Figure S5C and S5D). When injected with the mixture of all four MOs (PRL MOs), most embryos showed a clear phenotype, with severe shortening of the anterior-posterior axis and tortuous notochord (Figure 9B). Several other phenotypes were also observed after 24 hpf (Appendix 2A-2D). However, for further experiments, I focused at 24 hpf when the distinct phenotype was firstly observed. Short anterior-posterior axis is a typical phenotype caused by the defects in convergent extension, a developmental process involving the reorganization of embryonic epithelium (Wallingford et al., 2002). In this process, epithelial cells on the lateral sides of the embryo move towards the dorsal midline and intercalate with each other, and concomitantly the epithelial sheet extends along the anterior-posterior axis, dynamically changing the epithelial cell density at the dorsal side of the embryo (Tada and Heisenberg, 2012). *In situ* hybridization with *ntla* and *dlx3b*, markers for the notochord and neural plate border, respectively (Schulte-Merker et al., 1992; Akimenko et al., 1994), showed a short and wide notochord, with broader neural plate border, indicating a defect in convergent extension (Figure 9C). As progression of convergent extension requires appropriate cell density (Tada and Heisenberg, 2012), I

speculated that suppression of PRL increases the cell density of the epithelium, which in turn affects convergent extension. To visualize cells in the embryonic epithelium, I used transgenic zebrafish that express EGFP in the cells of the outermost periderm layer, and compared the cell density at 10 hpf when convergent extension completes. Embryos reached the tail-bud stage at 10 hpf, irrespective of the expression status of PRL, implying no overt effect on normal embryonic development. Epithelial cell density on the dorsal side of the embryos injected with PRL MOs increased slightly but significantly (Figure 9D and 9E). Immunostaining for anti-cleaved caspase-3 showed significant reduction in the number of positive cells in these embryos (Figure 9F and 9G). Altogether, these data implicate the role of PRL in regulating the epithelial cell density during convergent extension in zebrafish embryos, as in MDCK cell culture.

Discussion

In this study, I showed that PRL regulates epithelial cell density by inducing apoptosis at high cell density by upregulating the translation of E-cadherin, and subsequent activation of TGF-β pathway. These observations are consistent with previous studies that have reported E-cadherin-dependent activation of TGF-β pathway (Andl et al., 2006; Akieda et al., 2019) and cell death downstream of E-cadherin and TGF-β pathway (Lu et al., 2014; Akieda et al., 2019; Zhang et al., 2017). While several studies have shown the extrusion of dying cells from the epithelial sheet (Rosenblatt et al., 2001; Gu et al., 2011), what drives cell death and how it is regulated in apoptotic cell extrusion remain largely unknown. This study showed the importance of PRL in this process, and revealed the sequence of events involved in the induction of apoptosis downstream of PRL.

PRL is overexpressed in cancers and promotes cancer malignancy. Numerous studies have reported the increased expression of PRL, particularly at the advanced stages as compared to early stages of cancer (Saha et al., 2001; Polato et al., 2005; Radke et al., 2006; Dai et al., 2009; Mayinuer et al., 2013). This study identifies PRL as a regulator of epithelial cell density, and this may be a distinct function of PRL, particularly in non-transformed epithelia or at early stages of cancer. Such context-dependent multiple functions have also been reported for E-cadherin and TGF-β pathway. Although E-cadherin is widely known for its role in normal epithelia by physically joining cells and facilitating other juxtacrine signaling events (Gottardi et al., 2001), some studies suggest that E-cadherin expression in the late stage of cancer promotes invasion and distant metastasis, by enhancing the cancer cell survival in circulation, as well as by promoting

collective cell migration (Cheung et al., 2013; Padmanaban et al., 2019). Moreover, expression of E-cadherin during mesenchymal-to-epithelial transition (MET) at the sites of metastases is reported to promote the formation of metastatic tumors (Yao et al., 2011). In the case of TGF-β pathway, it has tumor suppressive effects in normal cells and in early-stage cancers, through inhibition of cell proliferation, induction of apoptosis, and inhibition of cell immortalization (Neel et al., 2012), but it promotes malignant progression in advanced stages of cancer probably due to genetic and epigenetic changes in the tumor cells, such as mutations in tumor suppressor p53 or loss of Smad4 (Adorno et al., 2009; Zhang et al., 2010).

One of the important questions that remain unanswered is the mechanism of PRL-induced upregulation of E-cadherin translation. It was recently reported that overexpression of Human antigen R (HuR), an RNA-binding protein (RBP), and suppression of CUG-binding protein 1 (CUGBP1), another RBP, both upregulate E-cadherin translation in Caco-2 cells (Yu et al., 2016). Both HuR and CUGBP1 interact directly with the 3′-untranslated region (3′-UTR) of *E-cadherin* mRNA; HuR prevents the translocation of mRNA to processing bodies, thereby increasing its accessibility to translation machinery, leading to upregulation of translation, while CUGBP1 promotes the translocation process and suppresses translation. However, overall regulation of E-cadherin translation remains poorly understood. Generally, the predominant regulation of mRNA translation is exerted at the initiation step (Sonenberg and Hinnebusch, 2009), which is normally facilitated by several eukaryotic translation initiation factors (eIFs) that are partly regulated by the mammalian target of rapamycin (mTOR) signaling (Ma and Blenis, 2009). Although mTOR is regarded as a critical regulator of global protein translation, several transcriptome-wide analyses of cell treated with mTOR inhibitors

have revealed that the translation of fewer than 600 mRNAs can be considered as extremely sensitive to mTOR (Hsieh et al., 2012; Larsson et al., 2012; Thoreen et al., 2012). This suggests that the regulation of the translation by mTOR is confined to specific mRNA populations. In the previous study, it was reported that overexpression of PRL stimulates mTOR signaling via inhibition of the Mg^{2+} transporter CNNM (Funato et al., 2014). Taken together, evidence suggests that PRL may promote E-cadherin translation by activating mTOR signaling. Several other mechanisms, including unwinding of secondary structures of the 5′-UTR by eIFs and binding of RBPs and/or poly(A)-binding proteins (PABPs) to the 3′-UTR, are also known to facilitate the translation of specific mRNA populations (Mignone et al., 2002; Sonenberg and Hinnebusch, 2009; Matoulkova et al., 2012; Burgess and Gray, 2010). Future studies, focusing on these factors responsible for the regulation of translation initiation, may help in understanding the mechanism of upregulation of E-cadherin translation by PRL.

PRL shows phosphatase activity towards certain substrates such as ezrin, phosphatidylinositol (4,5) bisphosphate, integrin β1, fizzy and cell division cycle 20 related 1 (FZR1), and PTEN (Forte et al., 2008; McParland et al., 2011; Tian et al., 2012; Zhang et al., 2019; Li et al., 2020). It also binds to CNNM Mg^{2+} transporters to regulate the level of intracellular Mg^{2+} (Funato et al., 2014; Hardy et al., 2015; Gulerez et al., 2016), which is crucial for various cellular signaling (Romani, 2011). In this study, dome formation was suppressed in the confluent cultures of cells expressing PRL, whereas cells that express the C104S mutant PRL, which has no phosphatase activity and no CNNM Mg^{2+} transporter-binding ability, were able to form domes, like control cells (Figure 1A). These results suggest the importance of at least one, if not both, of these two functions of PRL in regulating epithelial cell density. Studies using very recently identified PRL

C104D mutant, which lacks the phosphatase activity but has CNNM-binding ability (Kozlov et al., 2020), may identify the specific action of PRL that is essential to modulate the translation of E-cadherin. Future studies of PRL-mediated cell death at high cell density can be expected not only to reveal the details of cell-death mediated regulatory mechanism of epithelial cell density, but also broaden the understanding of the role of PRL in promoting cancer malignancy.

Materials and methods

Cell culture and transfection

MDCK cells were provided by Dr. Yasuyuki Fujita and Dr. Mihoko Kajita (Hokkaido University). MDCK-derived cell lines that express GFP-tagged PRL3 (PRL #1, PRL #2, and PRL C104S) in a Dox-inducible manner were established in the previous study (Kojima et al., 2019). The cells were routinely maintained in Dulbecco's modified Eagle's medium (DMEM; Nissui, 05919) supplemented with 10% fetal bovine serum (FBS) and antibiotics. For knockdown experiments, 3×10^5 cells were seeded in 35-mm dishes and cultured for 12 h. Cells were then transfected with siRNAs twice with a 24 h interval using Lipofectamine RNAiMAX (Invitrogen, 13778150). After 12 h, cells were trypsinized, re-seeded (1×10^6 cells) in other 35-mm dishes and cultured in the presence of Dox (2 μg/mL). The siRNA target sequences are as follows: *PRL1* siRNA #1, 5′-GCAACUUCUGUAUUUGGAGAAGUAU-3′; *PRL1* siRNA #2, 5′-CCAACCAAUGCGACCUUAAACAAAU-3′; *PRL2* siRNA #1, 5′-AUAUGUAGCAUCACAAACUCGAACC-3′; *PRL2* siRNA #2, 5′-GAGUGACAACUUUGGUUCGAGUUUG-3′; *E-cadherin* siRNA #1, 5′-UUGAUAGUGAACAUCAUGC-3′; *E-cadherin* siRNA #2, 5′-AGAAGAUACGGC AUGAGAG-3′; *Smad4* siRNA #1, 5′- AUGGCUGUCCCUCAAAGUC-3′; *Smad4* siRNA #2, 5′-AGUAACUCUGCACAAACAC-3′; negative control Lo GC siRNA (Invitrogen, 12935200).

Antibodies and chemicals

A rabbit anti-PRL antibody was generated in the previous study (Funato et al., 2014). Rabbit anti-ZO-1 antibody was a gift from Dr. Masahiko Itoh and Dr. Mikio Furuse (Furuse et al., 1994). Other commercially available primary antibodies used in this study were as follows: mouse monoclonal antibodies for β-actin (clone 2D4H5; Proteintech, 66009-1-Ig), β-catenin (clone 14; BD Bioscience, 610154), Na^+/K^+ ATPase (clone C464.6; Sigma-Aldrich, 05-369), 5-Bromo-2′-deoxy-uridine (BrdU) (clone BMG6H8; Roche, 11299964001), E-cadherin (clone 36; BD Bioscience, 610182) for immunoprecipitation analyses and staining MDCK cells, and Smad4 (clone B-8; Santa Cruz, sc-7966); rabbit monoclonal antibodies for Smad2 (clone D43B4; Cell signaling Technology, 5339), cleaved caspase-3 (clone 5A1E; Cell signaling Technology, 9664) for staining MDCK cells, and cleaved caspase-3 (clone C92-605; BD Bioscience, 559565) for staining zebrafish embryos; rat monoclonal antibodies for E-cadherin (clone ECCD2; Invitrogen, 13-1900) for immunoblotting analyses; and rabbit polyclonal antibodies for GFP (Invitrogen, A-11122). The secondary antibodies used in this study were as follows: Alexa-Fluor-568-conjugated anti-rabbit IgG (Invitrogen, A-11036) and Alexa-Fluor-568-conjugated anti-mouse IgG (Invitrogen, A-11031) for immunofluorescence staining and alkaline phosphatase (AP)-conjugated anti-rabbit IgG (Promega, S3731), AP-conjugated anti-rat IgG (Promega, S3831) and AP-conjugated anti-mouse IgG (Promega, S3721) for immunoblotting analyses. The inhibitors used in this study were as follows: cycloheximide (Sigma-Aldrich, 01810), ALK5 inhibitor II (Cayman, 14794), and SB525334 (Cayman, 16281). Recombinant Human TGF-β1 (R&D Systems, 240-B) was used for the stimulation of MDCK cells.

Transepithelial electrical resistance (TEER)

3.75×10^4 cells (equivalent to 1×10^6 cells in 35-mm dishes) were seeded on a membrane of transwell inserts (Corning, 3413) and cultured for 48 h after Dox treatment. Electrical resistance, across the epithelial sheet formed on the membrane, was measured using a Millicell-ERS device (Millipore) (Figure S6). Resistance of the blank membrane without cells was subtracted to obtain the actual resistance across the epithelial sheet. TEER was calculated by multiplying the resistance by the area of the membrane (0.33 cm^2) (Ωcm^2). The mean ± SD was obtained from three independent experiments.

Cell proliferation assay

Cells (1×10^6) were seeded on glass coverslips placed in 35-mm dishes and cultured for 12 h, and treated with Dox (2 μg/mL) for 24 or 48 h. Their proliferation status was determined using BrdU Labeling and Detection Kit II (Roche, 11299964001), according to the manufacturer's instructions. Briefly, cells were labeled with BrdU (3 μg/mL) for 30 min at 37˚C, fixed with 70% ethanol for 20 min at –20˚C, washed three times with phosphate-buffered saline (PBS), and incubated with anti-BrdU antibody for 30 min at 37˚C. After this, they were washed three times with PBS and then incubated with Alexa-Fluor-568-conjugated anti-mouse IgG antibody and 4′,6-diamidino-2-phenylindole (DAPI; Roche, 10236276001) for 30 min at room temperature (RT). Then, the cells were washed three times with PBS, and the glass coverslips were mounted on glass slides and observed under a confocal laser scanning microscope (FLUOVIEW FV1000, Olympus).

Immunofluorescence staining

Cells (1×10^6 or 2.5×10^5) were seeded in 35-mm dishes containing glass coverslips and

cultured for 12 h. They were treated with Dox (2 μg/mL) and cultured for 24 or 48 h. These cultured cells were then stained with anti-ZO-1 antibody, anti-β-catenin antibody, anti-Na^+/K^+ ATPase antibody, or anti-Smad2 antibody as described previously (Itoh et al., 1997; Hirata et al., 2014; Nallet-Staub et al., 2015), with a slight modification for anti-Smad2-staining. For this, cells were permeabilized with 0.1% TritonX-100 for 10 min at RT. For staining with anti-E-cadherin antibody (BD Bioscience), cells were fixed with 3.7% formaldehyde for 10 min on ice, washed three times with PBS, permeabilized and blocked with PBS containing 0.5% Triton X-100 and 5% normal goat serum for 1 h at RT. For staining with anti-cleaved caspase-3 antibody (Cell Signaling Technology), cells were fixed with 3.7% formaldehyde for 15 min at RT, washed three times with PBS, permeabilized and blocked with PBS containing 0.3% Triton X-100 and 5% BSA for 1 h at RT. Thereafter, the cells were incubated overnight with respective primary antibodies at 4˚C, followed by incubation with fluorophore-conjugated secondary antibodies, rhodamine-conjugated phalloidin (Wako, 165-21641), and DAPI for 30 min (for cleaved caspase-3 staining) or 1 h at RT. After washing the cells to remove excess antibody or stain, the glass coverslips were mounted on glass slides and observed under a confocal laser scanning microscope (FLUOVIEW FV1000).

Cytotoxicity assay

Cells (1×10^6) were seeded in 35-mm dishes and cultured with Dox (2 μg/mL) for 48 h. Cytotoxicity was determined by measuring the activity of LDH released from the cytosol of damaged cells, using a cytotoxicity LDH assay kit (Dojindo, CK12-05) according to the manufacturer's instructions. Briefly, culture medium was collected from dishes and centrifuged at 15,000 rpm for 10 min to remove cell debris. The resulting supernatant was

used to measure the activity of LDH released from the cells. To calculate the percentage of LDH release, the total LDH activity of the culture cells was also measured. For this, cells were lysed with 0.1% NP-40 in PBS, and the lysate was centrifuged at 15,000 rpm for 10 min. The resulting supernatant was used to measure total LDH activity. Finally, the percentage of LDH release was calculated by taking the ratio of the medium LDH activity to the total LDH activity.

Mechanical stretching of epithelial cell sheet

Polydimethylsiloxane (PDMS) membranes at the bottom of the wells of silicon chamber (Nepa Gene, NST-CH-4W) were coated with 0.01% poly-L-lysine. In each well, 2.9×10^5 cells (equivalent to 1×10^6 cells in 35-mm dishes) were seeded and cultured for 12 h, before treating them with Dox (2 μg/mL). After this, the silicon chamber was stretched by 20% and continued the culture for 24 h. The cells were fixed with 3.7% formaldehyde for 15 min at RT, and then the PDMS membranes were excised and used for immunofluorescence staining with anti-cleaved caspase-3 antibody.

Quantitative PCR (qPCR)

From the total RNA, extracted from cultured cells using RNAiso Plus (Takara, 9109), cDNA was synthesized, and analyzed by real-time PCR with Luna Universal One-Step RT-qPCR Kit (New England Biolabs, E3005). A MiniOpticon instrument (Bio-Rad) was used for monitoring fluorescence emitted by amplified DNA. Specific amplification during PCR was verified by agarose gel electrophoresis of the final PCR product from each experiment. The primer sets used were as follows: dog *E-cadherin*, 5′-AAGCGGCCTCTACAACTTCA-3′ and 5′-AACTGGGAAATGTGAGCACC-3′; dog

GAPDH, 5′-AACATCATCCCTGCTTCCAC-3′ and 5′-GACCACCTGGTCCTCAGTGT-3′.

Radiolabeling and immunoprecipitation

For radiolabeling, 6.4×10^6 cells (equivalent to 1×10^6 cells in 35-mm dishes) were seeded in 15-cm dishes. After 12 h, cells were treated with Dox (2 μg/mL) and cultured for further 48 h. They were preincubated in methionine- and cysteine-free medium (Gibco, 21013024), supplemented with glutamine and PBS-dialyzed 10% FBS for 30 min at 37˚C, before labeling with 200 μCi/mL of EasyTag™ EXPRESS^{35}S Protein Labeling Mix (Perkin Elmer, NEG772, 11 mCi/mL) for 30 min. They were lysed in RIPA buffer (150 mM NaCl, 50 mM Tris-HCl [pH 7.5], 1% deoxycholate, 0.1 % SDS, and 1 % Triton X-100) containing protease inhibitor cocktail (Roche, 04693159001). For immunoprecipitation, the total protein concentration of each lysate was estimated by Coomassie Brilliant Blue (CBB) staining. Equal amount of total protein from each lysate sample was incubated with mouse normal IgG (2 μg)-bound agarose beads for 1 h at 4˚C to remove non-specifically precipitated proteins (preclearing). The precleared lysates were subjected to immunoprecipitation with 10 μg of anti-E-cadherin antibody (BD Bioscience), and the precipitated proteins were separated by SDS-PAGE, immunoblotted with the same anti-E-cadherin antibody, and visualized by autoradiography.

Zebrafish maintenance

Zebrafish were raised and maintained according to internationally recognized guidelines (Westerfield, 2000). For this study, wild-type strain AB was used, along with a previously established transgenic line that expresses EGFP in the periderm (Tg [krt4p:gal4;

UAS:eGFP]), a gift from Dr. Kawakami and Dr. Wada (Wada et al., 2013). All experiments and animal care were according to the institutional and national guidelines and regulations (Osaka University, Permit #20005). Embryos and larvae were staged as described previously (Kimmel et al., 1995).

RNA sequencing

Zebrafish embryos were collected at the shield stage and tail-bud stage, which correspond to 6 hpf and 10 hpf, respectively. Total RNA was extracted with miRNeasy Mini Kit (Qiagen, 217004) according to the manufacturer's instructions. Libraries for sequencing were prepared with TruSeq stranded mRNA library prep kit (Illumina) according to the manufacturer's instructions. Paired-end sequencing on NovaSeq 6000 (Illumina) yielded 101 bp paired-end reads. Illumina Casava1.8.2 software was used for base calling. Sequenced reads were mapped to the zebrafish reference genome assembly (GRCz11) using TopHat v2.0.13 in combination with Bowtie2 ver. 2.2.3 and SAMtools ver. 0.1.19. The fragments per kilobase of exon per million mapped reads (FPKMs) were calculated using Cuffnorm version 2.2.1.

Microinjection of morpholino oligonucleotides (MOs) and mRNA into zebrafish embryo

For creating various knockdown embryos of zebrafish, following antisense MOs (Gene Tools) were used: *ptp4a1* MO, 5′-GGGCAGGUCUAUUCAUACGAGCCAU-3′; *ptp4a2a* MO, 5′-GGGCGAUUCAUUUUGACACUCAAAU-3′; *ptp4a2b variant 1* MO, 5′-CGUCCCAUUCAGGAGAAGAGUUUCU-3′; *ptp4a2b variant 2* MO, 5′-UCAACAGCGGCAGGGCGGUUCAU-3′; control MO, 5′-

CCUCUUACCUCAGUUACAAUUUAU-3′. For all injections, 1.7 ng of each MO was injected into one-cell stage embryos.

For mRNA microinjection, template plasmids were constructed. Briefly, total mRNA was extracted from one-cell staged zebrafish embryos using RNAiso Plus, and cDNA was synthesized using ReverTraAce (Toyobo, TRT-101). Approximately 100-bp-long 5′-UTR and 5′-ORF regions spanning the translation initiation site of the genes, namely, *ptp4a1*, *ptp4a2a*, *ptp4a2b variant 1*, and *ptp4a2b variant 2* (GeneBank accession numbers NM_001007775, NM_001005583, NM_001270540 and NM_001024098, respectively), which also contain the target sequence for each of the above four MOs, were amplified by PCR using zebrafish cDNA as template (schematically illustrated in Figure S5A). The primer sets used were as follows: zebrafish *ptp4a1*, 5′-GGGCTCGAGAGATTTTCAAGCTCTATTGCAAAG-3′ and 5′-GGGCTGCAGATTGTGGGTAATGAGGAATCTCA-3′; zebrafish *ptp4a2a*, 5′-GGGCTCGAGCCTGTAAAACAATCGGAAGTTGTTG-3′ and 5′-GGGCTGCAGCCTCATGCATTCATAAGTGATCTCA-3′; zebrafish *ptp4a2b variant 1 and 2*, 5′-GGGCTCGAGCTTCCTACAGATTTTTCTCCCTGTA-3′ for variant 1 and 5′-GGGCTCGAGTCTGAGCCAAAGATTTTTGAAAAGA-3′ for variant 2 and 5′-GGGCTGCAGATAGGAAATCTCAACAGCGGC-3′ for both variant 1 and 2. EGFP tag was transferred from the pEGFP-N1 vector into the pCS2 vector to construct pCS2-EGFP, and then each amplified PCR product was inserted in-frame into the C-terminus of EGFP. The plasmid constructs were then linearized, and transcribed *in vitro* using mMESSAGE mMACHINE™ SP6 Transcription Kit (ThermoFisher Scientific, AM1340) according to the manufacturer's instructions. Proper synthesis of each mRNA was verified by agarose gel electrophoresis. For all co-injection experiments with MOs, 100 pg of synthesized

mRNA was used.

Determination of peridermal cell density of zebrafish embryos

Embryos resulting from crossing the wild-type strain with that which shows periderm-specific GFP expression (Tg [krt4p:gal4; UAS:eGFP]) were injected with control MO or a combination of four MOs (PRL MOs: *ptp4a1* MO, *ptp4a2a* MO, *ptp4a2b variant 1* MO, and *ptp4a2b variant 2* MO). GFP-positive embryos were then selected at the tail-bud stage and fixed with 4% paraformaldehyde (PFA) overnight at 4˚C. The embryos were manually dechorionated with forceps, washed four times with 0.5% Triton X-100 in PBS, stained with DAPI, washed three times with 0.5% Triton X-100 in PBS, and observed under a confocal laser scanning microscope (FLUOVIEW FV3000). Images of horizontal sections taken at successive focal planes were stacked to generate three-dimensional images. Peridermal cell density was calculated by counting the number of nuclei per unit area.

Whole-mount immunostaining of zebrafish embryos

Embryos were fixed at the tail-bud stage with 4% PFA overnight at 4˚C. The dechorionated embryos were then washed four times with 0.5% Triton X-100 in PBS and blocked with 0.1% Triton X-100 in PBS containing 10% FBS and 1% dimethylsulfoxide (DMSO) for 1 h. Embryos were incubated overnight with anti-cleaved caspse-3 antibody (BD Bioscience) diluted in 0.01% Triton X-100 in PBS containing 1% FBS and 0.1% DMSO at 4˚C, and washed three times with 0.5% Triton X-100 in PBS. They were incubated overnight with Alexa-Fluor-568-conjugated secondary antibody and DAPI diluted in 0.1% Triton X-100 in PBS containing 1% DMSO at 4˚C. Images of stained

embryos were then acquired with a fluorescence stereo microscope (M205FA, Leica).

Whole-mount *in situ* hybridization of zebrafish embryo

Whole-mount *in situ* hybridization was performed as described previously (Shimizu et al., 2014). The images were acquired using a stereo microscope (M205A, Leica).

Statistical analyses

All statistical analyses were done with GraphPad Prism 6 software (GraphPad Software) and the data are presented as mean ± SEM. *p*-values were calculated by either Student's two-tailed *t*-test or one- or two-way ANOVA with post hoc test, as described in the figure legends.

Acknowledgements

I am greatly indebted to Prof. Hiroaki Miki for the continuous research guidance and invaluable feedbacks on my thesis. My sincere thanks also go to Dr. Yosuke Funato for the technical advice and helpful discussion on research topics. I am so grateful to Prof. Tohru Ishitani and Dr. Yuki Akieda (Department of Homeostatic Regulation, RIMD, Osaka University) who provided invaluable technical guidance on zebrafish research and also facilitated experiments. I also would like to thank Mr. Juqi Zou (Department of Homeostatic Regulation, RIMD, Osaka University) for the technical assistance during *in situ* hybridization experiment on zebrafish embryo. I would like to extend my sincere thanks to Dr. Kazuto Nunomura (Graduate School of Pharmaceutical Sciences, Osaka University) for the technical support on TEER measurement and Dr. Daisuke Okuzaki (Genome Information Research Center, RIMD, Osaka University) for the support on RNA sequencing analyses. I also take this opportunity to thank all members of Miki Lab for their kind support during my stay. I am also thankful to the Leading Graduate School Program: IPBS for the financial support and awarding research grant (Grant-in-Aid for Interdisciplinary Research 2020) which helped me concentrate on research work and provided an opportunity to expand the research scope. Finally, I would like to express profound gratitude to my parents and siblings for their continuous encouragement and all kind of support I needed throughout my graduate study.

References

Abercrombie, M., and Heaysman, J.E. (1954). Observations on the social behaviour of cells in tissue culture: II. “Monolayering” of fibroblasts. Exp. Cell Res. *6*, 293–306.

Adorno, M., Cordenonsi, M., Montagner, M., Dupont, S., Wong, C., Hann, B., Solari, A., Bobisse, S., Rondina, M.B., Guzzardo, V., et al. (2009). A Mutant-p53/Smad Complex Opposes p63 to Empower TGFβ-Induced Metastasis. Cell *137*, 87–98.

Akieda, Y., Ogamino, S., Furuie, H., Ishitani, S., Akiyoshi, R., Nogami, J., Masuda, T., Shimizu, N., Ohkawa, Y., and Ishitani, T. (2019). Cell competition corrects noisy Wnt morphogen gradients to achieve robust patterning in the zebrafish embryo. Nat. Commun. *10*, 4710.

Akimenko, M.A., Ekker, M., Wegner, J., Lin, W., and Westerfield, M. (1994). Combinatorial expression of three zebrafish genes related to distal-less: part of a homeobox gene code for the head. J. Neurosci. *14*, 3475–3486.

Andl, C.D., Fargnoli, B.B., Okawa, T., Bowser, M., Takaoka, M., Nakagawa, H., Klein-Szanto, A., Hua, X., Herlyn, M., and Rustgi, A.K. (2006). Coordinated functions of E-cadherin and transforming growth factor beta receptor II *in vitro* and *in vivo*. Cancer Res. *66*, 9878–9885.

Bai, Y., Zhou, H.M., Zhang, L., Dong, Y., Zeng, Q., Shou, W., and Zhang, Z.Y. (2016). Role of phosphatase of regenerating liver 1 (PRL1) in spermatogenesis. Sci. Rep. *6*, 34211.

Basak, S., Jacobs, S.B., Krieg, A.J., Pathak, N., Zeng, Q., Kaldis, P., Giaccia, A.J., and Attardi, L.D. (2008). The Metastasis-Associated Gene *Prl-3* Is a p53 Target Involved in Cell-Cycle Regulation. Mol. Cell *30*, 303–314.

Bessette, D.C., Qiu, D., and Pallen, C.J. (2008). PRL PTPs: mediators and markers of cancer progression. Cancer Metastasis Rev. *27*, 231–252.

Burgess, H.M., and Gray, N.K. (2010). mRNA-specific regulation of translation by poly(A)-binding proteins. Biochem. Soc. Trans. *38*, 1517–1522.

Cereijido, M., Ehrenfeld, J., Meza, I., and Martínez-Palomo, A. (1980). Structural and functional membrane polarity in cultured monolayers of MDCK cells. J. Membr. Biol. *52*, 147–159.

Cereijido, M., Ehrenfeld, J., Fernàndez-Castelo, S., and Meza, I. (1981). FLUXES, JUNCTIONS, AND BLISTERS IN CULTURED MONOLAYERS OF EPITHELIOID CELLS (MDCK). Ann. N. Y. Acad. Sci. *372*, 422–441.

Cheung, K.J., Gabrielson, E., Werb, Z., and Ewald, A.J. (2013). Collective Invasion in Breast Cancer Requires a Conserved Basal Epithelial Program. Cell *155*, 1639–1651.

Dai, N., Lu, A.P., Shou, C.C., and Li, J.Y. (2009). Expression of phosphatase regenerating liver 3 is an independent prognostic indicator for gastric cancer. World J. Gastroenterol. *15*, 1499–1505.

de Baaij, J.H., Stuiver, M., Meij, I.C., Lainez, S., Kopplin, K., Venselaar, H., Müller, D., Bindels, R.J., and Hoenderop, J.G. (2012). Membrane topology and intracellular processing of cyclin M2 (CNNM2). J. Biol. Chem. 287, 13644–13655.

Diamond, R.H., Cressman, D.E., Laz, T.M., Abrams, C.S., and Taub, R. (1994). PRL-1, a unique nuclear protein tyrosine phosphatase, affects cell growth. Mol. Cell Biol. *14*, 3752-3762.

Dong, Y., Zhang, L., Zhang, S., Bai, Y., Chen, H., Sun, X., Yong, W., Li, W., Colvin, S. C., Rhodes, S. J., et al. (2012). Phosphatase of regenerating liver 2 (PRL2) is essential for placental development by down-regulating PTEN (Phosphatase and Tensin Homologue Deleted on Chromosome 10) and activating Akt protein. J. Biol. Chem. *287*, 32172–32179.

Dong, Y., Zhang, L., Bai, Y., Zhou, H.M., Campbell, A.M., Chen, H., Yong, W., Zhang, W., Zeng, Q., Shou, W., et al. (2014). Phosphatase of Regenerating Liver 2 (PRL2) Deficiency Impairs Kit Signaling and Spermatogenesis. J. Biol. Chem. *289*, 3799–3810.

Dumaual, C.M., Sandusky, G.E., Crowell, P.L., and Randall, S.K. (2006). Cellular Localization of PRL-1 and PRL-2 Gene Expression in Normal Adult Human Tissues. J.

Histochem. Cytochem. *54*, 1401-1412.

Eagle, H., and Levine, E.M. (1967). Growth Regulatory Effects of Cellular Interaction. Nature *213*, 1102–1106.

Eisenhoffer, G.T., Loftus, P.D., Yoshigi, M., Otsuna, H., Chien, C.B., Morcos, P.A., and Rosenblatt, J. (2012). Crowding induces live cell extrusion to maintain homeostatic cell numbers in epithelia. Nature *484*, 546–549.

Forte, E., Orsatti, L., Talamo, F., Barbato, G., De Francesco, R., and Tomei, L. (2008). Ezrin is a specific and direct target of protein tyrosine phosphatase PRL-3. Biochim. Biophys. Acta. *1783*, 334–344.

Funato, Y., Yamazaki, D., Mizukami, S., Du, L., Kikuchi, K., and Miki, H. (2014). Membrane protein CNNM4-dependent Mg^{2+} efflux suppresses tumor progression. J. Clin. Invest. *124*, 5398–5410.

Funato, Y., Yoshida, A., Hirata, Y., Hashizume, O., Yamazaki, D., and Miki, H. (2020). The Oncogenic PRL Protein Causes Acid Addiction of Cells by Stimulating Lysosomal Exocytosis. Dev. Cell *55*, 387–397.e8.

Furuse, M., Itoh, M., Hirase, T., Nagafuchi, A., Yonemura, S., Tsukita, S., and Tsukita, S. (1994). Direct association of occludin with ZO-1 and its possible involvement in the localization of occludin at tight junctions. J. Cell Biol. *127*, 1617–1626.

Gottardi, C.J., Wong, E., and Gumbiner, B.M. (2001). E-Cadherin Suppresses Cellular Transformation by Inhibiting β-Catenin Signaling in an Adhesion-Independent Manner. J. Cell Biol. *153*, 1049–1060.

Gu, Y., Forostyan, T., Sabbadini, R., and Rosenblatt, J. (2011). Epithelial cell extrusion requires the sphingosine-1-phosphate receptor 2 pathway. J. Cell Biol. *193*, 667–676.

Gulerez, I., Funato, Y., Wu, H., Yang, M., Kozlov, G., Miki, H., and Gehring, K. (2016). Phosphocysteine in the PRL-CNNM pathway mediates magnesium homeostasis. EMBO Rep. *17*, 1890–1900.

Guo, K., Li, J., Tang, J.P., Koh, V., Gan, B.Q., and Zeng, Q. (2004). Catalytic domain of PRL-3 plays an essential role in tumor metastasis: formation of PRL-3 tumors inside the blood vessels. Cancer Biol. Ther. *3*, 945–951.

Guo, P., Xu, X., Wang, F., Yuan, X., Tu, Y., Zhang, B., Zheng, H., Yu, D., Ge, W., Gong, Z., et al. (2019). A Novel Neuroprotective Role of *Phosphatase of Regenerating Liver-1* against CO2 Stimulation in Drosophila. iScience *19,* 291-302.

Hardy, S., Uetani, N., Wong, N., Kostantin, E., Labbé, D.P., Bégin, L.R., Mes-Masson, A., Miranda-Saavedra, D., and Tremblay, M.L. (2015). The protein tyrosine phosphatase PRL-2 interacts with the magnesium transporter CNNM3 to promote oncogenesis. Oncogene *34*, 986–995.

Hardy, S., Kostantin, E., Hatzihristidis, T., Zolotarov, Y., Uetani, N., and Tremblay, M.L. (2018). Physiological and oncogenic roles of the PRL phosphatases. FEBS J. *285*, 3886-3908.

Hirata, Y., Funato, Y., and Miki, H. (2014). Basolateral sorting of the Mg^{2+} transporter CNNM4 requires interaction with AP-1A and AP-1B. Biochem. Biophys. Res. Commun. *455*, 184–189.

Hsieh, A.C., Liu, Y., Edlind, M.P., Ingolia, N.T., Janes, M.R., Sher, A., Shi, E.Y., Stumpf, C.R., Christensen, C., Bonham, M.J., Wang, S., et al. (2012). The translational landscape of mTOR signalling steers cancer initiation and metastasis. Nature *485*, 55–61.

Ichida, J.K., Blanchard, J., Lam, K., Son, E.Y., Chung, J.E., Egli, D., Loh, K.M., Carter, A.C., Di Giorgio, F.P., Koszka, K., et al. (2009). A Small-Molecule Inhibitor of Tgf-β Signaling Replaces *Sox2* in Reprogramming by Inducing *Nanog*. Cell Stem Cell *5*, 491–503.

Itoh, M., Nagafuchi, A., Moroi, S., and Tsukita, S. (1997). Involvement of ZO-1 in Cadherin-based Cell Adhesion through Its Direct Binding to α Catenin and Actin Filaments. J. Cell Biol. *138*, 181–192.

Johansson, J.A., Marie, K.L., Lu, Y., Brombin, A., Santoriello, C., Zeng, Z., Zich, J., Gautier, P., von Kriegsheim, A., Brunsdon, H., et al. (2020). PRL3-DDX21 Transcriptional Control of Endolysosomal Genes Restricts Melanocyte Stem Cell

Differentiation. Dev Cell. *54*, 317-332.e9.

Kimmel, C.B., Ballard, W.W., Kimmel, S.R., Ullmann, B., and Schilling, T.F. (1995). Stages of Embryonic Development of the Zebrafish. Dev. Dyn. *203*, 253–310.

Kojima, T., Funato, Y., and Miki, H. (2019). Phosphatase of regenerating liver sensitizes MET to functional activation by hepatocyte growth factor. Biochem. J. *476*, 1419–1431.

Kozlov, G., Cheng, J., Ziomek, E., Banville, D., Gehring, K., and Ekiel, I. (2004). Structural Insights into Molecular Function of the Metastasis-associated Phosphatase PRL-3. J. Biol. Chem. *279*, 11882–11889.

Kozlov, G., Funato, Y., Chen, Y.S., Zhang, Z., Illes, K., Miki, H., and Gehring, K. (2020). PRL3 pseudophosphatase activity is necessary and sufficient to promote metastatic growth. J. Biol. Chem. *295*, 11682–11692.

Laping, N.J., Everitt, J.I., Frazier, K.S., Burgert, M., Portis, M.J., Cadacio, C., Gold, L.I., and Walker, C.L. (2007). Tumor-Specific Efficacy of Transforming Growth Factor-βRI Inhibition in Eker Rats. Clin. Cancer Res. *13*, 3087–3099.

Larsson, O., Morita, M., Topisirovic, I., Alain, T., Blouin, M.J., Pollak, M., and Sonenberg, N. (2012). Distinct perturbation of the translatome by the antidiabetic drug metformin. Proc. Natl. Acad. Sci. *109*, 8977–8982.

Leighton, J., Brada, Z., Estes, L. W., and Justh, G. (1969). Secretory Activity and Oncogenicity of a Cell Line (MDCK) Derived from Canine Kidney. Science *163*, 472–473.

Li, Q., Bai, Y., Lyle, L.T., Yu, G., Amarasinghe, O., Nguele Meke, F., Carlock, C., and Zhang, Z.Y. (2020). Mechanism of PRL2 phosphatase-mediated PTEN degradation and tumorigenesis. Proc. Natl. Acad. Sci. *117*, 20538–20548.

Liu, F., Pouponnot, C., and Massagué, J. (1997). Dual role of the Smad4/DPC4 tumor suppressor in TGFβ-inducible transcriptional complexes. Genes Dev. *11*, 3157–3167.

Lu, M., Marsters, S., Ye, X., Luis, E., Gonzalez, L., and Ashkenazi, A. (2014). E-Cadherin Couples Death Receptors to the Cytoskeleton to Regulate Apoptosis. Mol. Cell *54*, 987–998.

Ma, S., Meng, Z., Chen, R., and Guan, K.L. (2019). The Hippo Pathway: Biology and Pathophysiology. Annu. Rev. Biochem. *88*, 577–604.

Ma, X.M., and Blenis, J. (2009). Molecular mechanisms of mTOR-mediated translational control. Nat. Rev. Mol. Cell Biol. *10*, 307–318.

Marinari, E., Mehonic, A., Curran, S., Gale, J., Duke, T., and Baum, B. (2012). Live-cell delamination counterbalances epithelial growth to limit tissue overcrowding. Nature *484*, 542–545.

Matoulkova, E., Michalova, E., Vojtesek, B., and Hrstka, R. (2012). The role of the 3' untranslated region in post-transcriptional regulation of protein expression in mammalian cells. RNA Biol. *9*, 563–576.

Matter, W.F., Estridge, T., Zhang, C., Belagaje, R., Stancato, L., Dixon, J., Johnson, B., Bloem, L., Pickard, T., Donaghue, M., et al. (2001). Role of PRL-3, a Human Muscle-Specific Tyrosine Phosphatase, in Angiotensin-II Signaling. Biochem. Biophys. Res. Commun. *283*, 1061-1068.

Mayinuer, A., Yasen, M., Mogushi, K., Obulhasim, G., Xieraili, M., Aihara, A., Tanaka, S., Mizushima, H., Tanaka, H., and Arii, S. (2013). Upregulation of Protein Tyrosine Phosphatase Type IVA Member 3 (PTP4A3/PRL-3) is Associated with Tumor Differentiation and a Poor Prognosis in Human Hepatocellular Carcinoma. Ann. Surg. Oncol. *20*, 305–317.

McClatchey, A.I., and Yap, A.S. (2012). Contact inhibition (of proliferation) redux. Curr. Opin. Cell Biol. *24*, 685–694.

McCrea, P.D., Turck, C.W., and Gumbiner, B. (1991). A homolog of the armadillo protein in Drosophila (plakoglobin) associated with E-cadherin. Science *254*,1359–1361.

McParland, V., Varsano, G., Li, X., Thornton, J., Baby, J., Aravind, A., Meyer, C., Pavic, K., Rios, P., and Köhn, M. (2011). The Metastasis-Promoting Phosphatase PRL-3 Shows Activity toward Phosphoinositides. Biochemistry *50*, 7579–7590.

Mignone, F., Gissi, C., Liuni, S., and Pesole, G. (2002). Untranslated regions of mRNAs. Genome Biol. *3*, reviews0004.1– reviews0004.10.

Misfeldt, D.S., Hamamoto, S.T., and Pitelka, D.R. (1976). Transepithelial transport in cell culture. Proc. Natl. Acad. Sci. *73*, 1212–1216.

Nallet-Staub, F., Yin, X., Gilbert, C., Marsaud, V., Ben Mimoun, S., Javelaud, D., Leof, E. B., and Mauviel, A. (2015). Cell Density Sensing Alters TGF-β Signaling in a Cell-Type-Specific Manner, Independent from Hippo Pathway Activation. Dev. Cell *32*, 640–651.

Neel, J.C., Humbert, L., and Lebrun, J.J. (2012). The Dual Role of TGFβ in Human Cancer: From Tumor Suppression to Cancer Metastasis. ISRN Mol. Biol. *2012*, 381428.

Padmanaban, V., Krol, I., Suhail, Y., Szczerba, B.M., Aceto, N., Bader, J.S., and Ewald, A.J. (2019). E-cadherin is required for metastasis in multiple models of breast cancer. Nature *573*, 439–444.

Pagarigan, K.T., Bunn, B.W., Goodchild, J., Rahe, T.K., Weis, J.F., and Saucedo, L.J. (2013). *Drosophila* PRL-1 Is a Growth Inhibitor That Counteracts the Function of the Src Oncogene. PLoS One *8*, e61084.

Polato, F., Codegoni, A., Fruscio, R., Perego, P., Mangioni, C., Saha, S., Bardelli, A., and Broggini, M. (2005). PRL-3 Phosphatase Is Implicated in Ovarian Cancer Growth. Clin.

Cancer Res. *11*, 6835–6839.

Radke, I., Götte, M., Kersting, C., Mattsson, B., Kiesel, L., and Wülfing, P. (2006). Expression and prognostic impact of the protein tyrosine phosphatases PRL-1, PRL-2, and PRL-3 in breast cancer. Br. J. Cancer *95*, 347–354.

Romani, A.M. (2011). CELLULAR MAGNESIUM HOMEOSTASIS. Arch. Biochem. Biophys. *512*, 1–23.

Rosenblatt, J., Raff, M.C., and Cramer, L.P. (2001). An epithelial cell destined for apoptosis signals its neighbors to extrude it by an actin- and myosin-dependent mechanism. Curr. Biol. *11*, 1847–1857.

Saha, S., Bardelli, A., Buckhaults, P., Velculescu, V.E., Rago, C., St Croix, B., Romans, K.E., Choti, M.A., Lengauer, C., Kinzler, K.W., et al. (2001). A Phosphatase Associated with Metastasis of Colorectal Cancer. Science *294*, 1343–1346.

Schulte-Merker, S., Ho, R.K., Herrmann, B.G., and Nüsslein-Volhard, C. (1992). The protein product of the zebrafish homologue of the mouse T gene is expressed in nuclei of the germ ring and the notochord of the early embryo. Development *116*, 1021–1032.

Shi, Y., and Massagué, J. (2003). Mechanisms of TGF-β Signaling from Cell Membrane to the Nucleus. Cell *113*, 685–700.

Shimizu, N., Ishitani, S., Sato, A., Shibuya, H., and Ishitani, T. (2014). Hipk2 and PP1c cooperate to maintain Dvl protein levels required for Wnt signal transduction. Cell Rep. *8*, 1391–1404.

Skou, J.C. (1957). The Influence of Some Cations on an Adenosine Triphosphatase from Peripheral Nerves. Biochim. Biophys. Acta. *23*, 394–401.

Sonenberg, N., and Hinnebusch, A.G. (2009). Regulation of Translation Initiation in Eukaryotes: Mechanisms and Biological Targets. Cell *136*, 731–745.

Srinivasan, B., Kolli, A.R., Esch, M.B., Abaci, H.E., Shuler, M.L., and Hickman, J.J. (2015). TEER Measurement Techniques for In Vitro Barrier Model Systems. J. Lab. Autom. *20*, 107–126.

Stevenson, B.R., Siliciano, J.D., Mooseker, M.S., and Goodenough, D.A. (1986). Identification of ZO-1: a high molecular weight polypeptide associated with the tight junction (zonula occludens) in a variety of epithelia. J. Cell Biol. *103*, 755–766.

Sun, J.P., Wang, W.Q., Yang, H., Liu, S., Liang, F., Fedorov, A.A., Almo, S.C., and Zhang, Z.Y. (2015). Structure and Biochemical Properties of PRL-1, a Phosphatase Implicated in Cell Growth, Differentiation, and Tumor Invasion. Biochemistry *44*, 12009-12021.

Tada, M., and Heisenberg, C.P. (2012). Convergent extension: using collective cell migration and cell intercalation to shape embryos. Development *139*, 3897–3904.

Takeichi, M. (1977). Functional correlation between cell adhesive properties and some cell surface proteins. J. Cell Biol. *75*, 464–474.

Thoreen, C.C., Chantranupong, L., Keys, H.R., Wang, T., Gray, N.S., and Sabatini, D.M. (2012). A unifying model for mTORC1-mediated regulation of mRNA translation. Nature *485*, 109–113.

Tian, W., Qu, L., Meng, L., Liu, C., Wu, J., and Shou, C. (2012). Phosphatase of regenerating liver-3 directly interacts with integrin β1 and regulates its phosphorylation at tyrosine 783. BMC Biochem. *13*, 22.

Tonks, N.K. (2006). Protein tyrosine phosphatases: from genes, to function, to disease. Nat. Rev. Mol. Cell Biol. *7*, 833-846.

Wada, H., Ghysen, A., Asakawa, K., Abe, G., Ishitani, T., and Kawakami, K. (2013). Wnt/Dkk negative feedback regulates sensory organ size in zebrafish. Curr. Biol. *23*, 1559-1565.

Wallingford, J.B., Fraser, S.E., and Harland, R.M. (2002). Convergent Extension: The Molecular Control of Polarized Cell Movement during Embryonic Development. Dev. Cell *2*, 695–706.

Wei, M., Korotkov, K.V., and Blackburn, J.S. (2018). Targeting phosphatases of

regenerating liver (PRLs) in cancer. Pharmacol. Ther. *190*, 128-138.

Westerfield, M. (2000). The zebrafish book. A guide for the laboratory use of zebrafish (Danio rerio). 4th ed., Univ. of Oregon Press, Eugene.

Yao, D., Dai, C., and Peng, S. (2011). Mechanism of the Mesenchymal–Epithelial Transition and Its Relationship with Metastatic Tumor Formation. Mol. Cancer Res. *9*, 1608–1620.

Yu, L., Kelly, U., Ebright, J.N., Malek, G., Saloupis, P., Rickman, D.W., McKay, B.S., Arshavsky, V.Y., and Bowes Rickman, C. (2007). Oxidative Stress-Induced Expression and Modulation of Phosphatase of Regenerating Liver-1 (PRL-1) in Mammalian Retina. Biochim. Biophys. Acta. *1773*, 1473-1482.

Yu, T.X., Gu, B.L., Yan, J.K., Zhu, J., Yan, W.H., Chen, J., Qian, L.X., and Cai, W. (2016). CUGBP1 and HuR regulate E-cadherin translation by altering recruitment of E-cadherin mRNA to processing bodies and modulate epithelial barrier function. Am. J. Physiol. Cell Physiol. *310*, C54–C65.

Zeng, Q., Hong, W., and Tan, Y.H. (1998). Mouse PRL-2 and PRL-3, Two Potentially Prenylated Protein Tyrosine Phosphatases Homologous to PRL-1. Biochem. Biophys. Res. Commun. *244*, 421–427.

Zeng, Q., Si, X., Horstmann, H., Xu, Y., Hong, W., and Pallen, C.J. (2000). Prenylation-

dependent association of protein-tyrosine phosphatases PRL-1, -2, and -3 with the plasma membrane and the early endosome. J. Biol. Chem. *275*, 21444-21452.

Zhang, B., Halder, S.K., Kashikar, N.D., Cho, Y.J., Datta, A., Gorden, D.L., and Datta, P.K. (2010). Antimetastatic Role of Smad4 Signaling in Colorectal Cancer. Gastroenterology *138*, 969–980.e3.

Zhang, C., Qu, L., Lian, S., Meng, L., Min, L., Liu, J., Song, Q., Shen, L., and Shou, C. (2019). PRL-3 Promotes Ubiquitination and Degradation of AURKA and Colorectal Cancer Progression via Dephosphorylation of FZR1. Cancer Res. *79*, 928–940.

Zhang, Y., Alexander, P.B., and Wang, X.F. (2017). TGF-β Family Signaling in the Control of Cell Proliferation and Survival. Cold Spring Harb. Perspect. Biol. *9*, a022145.

Zhao, B., Wei, X., Li, W., Udan, R.S., Yang, Q., Kim, J., Xie, J., Ikenoue, T., Yu, J., Li, L., et al. (2007). Inactivation of YAP oncoprotein by the Hippo pathway is involved in cell contact inhibition and tissue growth control. Genes Dev. *21*, 2747–2761.

Zhao, B., Ye, X., Yu, J., Li, L., Li, W., Li, S., Yu, J., Lin, J.D., Wang, C.Y., Chinnaiyan, A.M., et al. (2008). TEAD mediates YAP-dependent gene induction and growth control. Genes Dev. *22*, 1962–1971.

Zimmerman, M.W., Homanics, G.E., and Lazo, J.S. (2013). Targeted Deletion of the Metastasis-Associated Phosphatase *Ptp4a3* (PRL-3) Suppresses Murine Colon Cancer.

PLoS One. *8*, e58300.

Figure Legends

Figure 1. Schematic illustration showing membrane anchored-PRL.

PRL consists of the catalytic protein tyrosine phosphatase (PTP) domain on its N-terminal end and the prenylation domain on its C-terminal end. The prenylation is important for the membrane anchoring of PRL.

Figure 2. Schematic illustration showing the interaction of PRL with Mg^{2+} transporter CNNM.

CNNM extrudes Mg^{2+} from the cell by exchanging it with Na^{+} (left). PRL interacts with intracellular CBS domain of CNNM, and inhibits the ion transport (right).

Figure 3. Schematic illustration showing phenotypes of *Prl*-KO mice.

Prl1-KO or *Prl3*-KO mice showed no observable phenotypic alterations and *Prl2*-KO mice showed only mild phenotypes such as growth retardation and reduced fertility (top). Double KO for *Prl1* and *Prl2* were found to be embryonic lethal (bottom).

Figure 4. PRL expression suppresses dome formation at confluence.

(A, B) Indicated cells (1×10^6 cells for A, and 2×10^6 cells for B) were seeded in 35-mm dishes and cultured with (+) or without (–) Dox for 48 h. Phase-contrast images of each cell line are shown. Arrowheads indicate round and swollen structures. The number of swollen structures per cm^2 is also indicated. Scale bar, 400 μm.

(C) Cells were stained with phalloidin (red) and DAPI (blue). Images of horizontal section

(XY) were acquired using a confocal microscope and those of vertical section (XZ) were reconstituted from the stack of the multiple XY images. Vertical sections were taken at the white dotted lines shown in the XY images. The center dark regions in the XY images of control cells and PRL #1 cells (− Dox) represent the internal part of domes. Scale bar, 25 μm.

Figure 5. PRL expression lowers the cell density of epithelial sheet.

(A) Indicated cells (1×10^6 cells) were seeded in 35-mm dishes and cultured with (+) or without (–) Dox for 48 h. Cells were stained with DAPI, and observed under confocal microscope. Scale bar, 10 μm.

(B) Indicated numbers of cells were seeded, cultured, and stained as in (A). The graph shows the number of nuclei per mm^2 (mean ± SEM, n = 20). The *p* values were determined by two-way ANOVA with Holm-Sidak's post hoc test. $^{****}p < 0.0001$, N.S.: not-significant.

(C) Indicated cells were seeded and cultured as in (A). The graph shows the percentage of LDH release from the cells (mean ± SEM, n = 3). The *p* values were determined by two-way ANOVA followed by Holm-Sidak's post hoc test. $^{*}p < 0.05$.

(D-F) Indicated cells were seeded at either high density (1×10^6 cells, D) or low density (2.5×10^5 cells, E) in 35-mm dishes and cultured with (+) or without (–) Dox for 24 h. Cells were stained with anti-cleaved caspase3 antibody (red) and DAPI (blue), and observed under confocal microscope (D, E). The signal of GFP (green) is also shown. Scale bar, 100 μm. The graph (F) shows the percentage of cells positive for cleaved caspase-3 (mean ± SEM, n = 30). The *p* values were determined by two-way ANOVA with Holm-Sidak's post hoc test. $^{****}p < 0.0001$.

(G) Schematic illustration showing mechanical stretch of epithelial cell sheet cultured in silicon chamber.

(H, I) Indicated cells were treated with Dox and epithelial cell sheet was stretched as in (G). The cells were stained with anti-cleaved caspase-3 antibody (red) and DAPI (blue), and observed under confocal microscope (H). The signal of GFP (green) is also shown. Scale bar, 100 μm. The graph (I) shows the percentage of cells positive for cleaved caspase-3 (mean ± SEM, n = 30). The *p* values were determined by two-way ANOVA with Holm-Sidak's post hoc test. $^{****}p < 0.0001$, N.S.: not-significant.

Figure 6. Knockdown of PRL1 or PRL2 reduces cell death and increases cell density.

(A, B) MDCK cells were transfected with *PRL1* siRNA (#1 or #2) or *PRL2* siRNA (#1 or #2). Cell lysates were collected 48 h after Dox treatment and immunoblotted with indicated antibodies (A). Cells were stained with anti-cleaved caspase-3 antibody and DAPI, and observed under confocal microscope (B). Scale bar, 100 μm.

(C) The graph shows the percentage of cells positive for cleaved caspase-3 (mean ± SEM, n = 30 to 100). The *p* values were determined by one-way ANOVA with Sidak's post hoc test. $^{****}p < 0.0001$.

(D) The graph shows the number of nuclei per mm^2 (mean ± SEM, n = 30 to 100). The *p* values were determined by one-way ANOVA with Sidak's post hoc test. $^{*}p < 0.05$, $^{***}p < 0.001$ $^{****}p < 0.0001$.

Figure 7. Increased E-cadherin expression is necessary for driving cell death

(A) Indicated cells were cultured with Dox for 48 h, and cell lysates were immunoblotted with the indicated antibodies.

(B-D) Indicated cells were transfected with *E-cadherin* siRNA (#1 or #2). Cell lysates were harvested 24 h after Dox treatment, and immunoblotted with indicated antibodies (B) or immunostained with anti-cleaved caspase-3 antibody (C). Scale bar, 100 μm. The graph (D) shows the percentage of cells positive for cleaved caspase-3 (mean ± SEM, n = 15). The *p* values were determined by two-way ANOVA with Holm-Sidak's post hoc test. $^{****}p < 0.0001$, N.S.: not-significant.

(E-G) Indicated cells were radiolabeled with [^{35}S]methionine and [^{35}S]cysteine for 30 min and cell lysates were immunoblotted with indicated antibodies or autoradiographed (^{35}S) (E). The cell lysates were immunoprecipitated with anti-E-cadherin antibody, followed by immunoblotting with anti-E-cadherin antibody or autoradiography (^{35}S) (F). The graph (G) shows relative levels of S^{35}-labelled E-cadherin in the immunoprecipitates (mean ± SEM, n = 3). The *p* values were determined by two-tailed Student's *t*-test. $^{*}p < 0.05$.

Figure 8. TGF-β pathway drives cell death downstream of E-cadherin.

(A, B) Indicated cells were cultured with Dox for 24 h, and stimulated with (+) TGF-β (10 ng/mL) for 30 min or without (–) stimulation. Cells were stained with anti-Smad2 antibody, and observed under confocal microscope (A). Scale bar, 10 μm. The graph (B) shows the ratio of nuclear to cytoplasmic (Nuc/ Cyto) Smad2 signal (mean ± SEM, n = 16 to 20). The *p* values were determined by one-way ANOVA with Sidak's post hoc test. $^{****}p < 0.0001$.

(C, D) Indicated cells were transfected with *E-cadherin* siRNA (#1 or #2), fixed 24 h after Dox treatment, and immunostained with anti-Smad2 antibody (C). Scale bar, 10 μm. The graph (D) shows the ratio of nuclear to cytoplasmic (Nuc/ Cyto) Smad2 signal (mean ± SEM, n = 20). The *p* values were determined by one-way ANOVA with Sidak's post hoc

test. $^{***}p < 0.001$, $^{****}p < 0.0001$.

(E, F) Indicated cells were cultured with Dox and ALK5 inhibitors, ALK5 inhibitor II (10 μM) or SB525334 (5 μM), for 24 h, stained with anti-cleaved caspase-3 antibody, and observed under confocal microscope (E). Scale bar, 100 μm. The graph (F) shows the percentage of cells positive for cleaved caspase-3 (mean ± SEM, n = 20 to 55). The *p* values were determined by one-way ANOVA with Sidak's post hoc test. $^{****}p < 0.0001$.

(G-I) Indicated cells were transfected with *Smad4* siRNA (#1 or #2), harvested or fixed 24 h after Dox treatment, and immunoblottied with indicated antibodies (G) or immunostained with anti-cleaved caspase-3 antibody (H), respectively. Scale bar, 100 μm. The graph (I) shows the percentage of cells positive for cleaved caspase-3 (mean ± SEM, n = 22). The *p* values were determined by one-way ANOVA with Sidak's post hoc test. $^{****}p < 0.0001$.

Figure 9. PRL controls epithelial cell density and convergent extension in zebrafish embryos.

(A) RNA sequencing of wild-type zebrafish embryos. The data shows the mRNA level of zebrafish PRL isoforms (*ptp4a1*, *ptp4a2a*, *ptp4a2b*, *ptp4a3a*, and *ptp4a3b*) at 6 hpf and 10 hpf. Expression levels, normalized in fragments per kilobase of exon per million mapped reads (FPKM), are indicated by the gradient of color.

(B) One-cell stage zebrafish embryos were injected with 6.8 ng of control MO or combination of MOs targeting four PRL isoforms (PRL MOs; *ptp4a1* MO, *ptp4a2a* MO, *ptp4a2b variant 1* MO, and *ptp4a2b variant 2* MO). Phase-contrast images of 24 hpf zebrafish larvae with the percentage of those with abnormal morphologies are shown (left). Scale bar, 250 μm. Magnified images of the boxed areas are also shown (right) and

the white dotted lines outline the notochord.

(C) Zebrafish embryos were injected with indicated MOs, and tail-bud stage embryos were used for whole-mount *in situ* hybridization for *ntla* and *dlx3b*. The percentage of embryos with abnormal morphologies are also shown. A and P indicate anterior and posterior sides of the embryo, respectively. Scale bar, 150 μm.

(D, E) Tg [krt4p:gal4; UAS:eGFP] zebrafish embryos were injected with indicated MOs, and at tail-bud stage, the dorsal periderm was observed for GFP fluorescence (D). Scale bar, 20 μm. The graph (E) shows the number of nuclei per mm^2 (mean ± SEM, n =12 to 15). The *p* values were determined by two-tailed Student's *t*-test. $^{*}p < 0.05$.

(F, G) Zebrafish embryos injected with indicated MOs were stained with anti-cleaved caspase-3 antibody at tail-bud stage (F). A and P indicate the anterior and posterior sides of the embryo, respectively. Scale bar, 200 μm. The graph (G) shows the number of cells positive for cleaved caspase-3 per mm^2 (mean ± SEM, n =25 to 26). The *p* values were determined by two-tailed Student's *t*-test. $^{****}p < 0.0001$.

Figure S1. PRL expression does not affect apicobasal polarity in MDCK cells.

Indicated cells (1×10^6 cells) were seeded in 35-mm dishes and cultured with Dox for 48 h. Cells were stained with indicated antibodies (red) and DAPI (blue). Images of horizontal section (XY) and vertically reconstituted images (XZ) are shown. Vertical sections were taken at the white dotted lines indicated in the XY images. Scale bar, 10 μm.

Figure S2. PRL expression does not suppress cell proliferation at confluence.

(A, B) Indicated cells (1×10^6 cells) were seeded in 35-mm dishes and cultured with (+)

or without (–) Dox for indicated time. Cells were labelled with BrdU and stained with anti-BrdU antibody (red) and DAPI (blue) (A). Scale bar, 40 μm. The graph (B) shows the percentage of cells positive for BrdU (mean ± SEM, n = 20).

Figure S3. Double knockdown for PRL1 and PRL2 damages the cell culture.

MDCK cells were transfected with both *PRL1* siRNA #1 and *PRL2* siRNA #2. Cells were stained with DAPI and observed under confocal microscope. Scale bar, 100 μm.

Figure S4. PRL expression does not augment *E-cadherin* mRNA levels and E-cadherin protein stability.

(A) Indicated cells were cultured with Dox for 48 h. Cells were collected and mRNA levels were measured by quantitative PCR. The graph shows relative *E-cadherin* mRNA levels normalized to those of *GAPDH* (mean ± SEM, n = 8). The *p* values were determined by two-tailed Student's *t*-test. N.S.: not-significant.

(B, C) Indicated cell lines (1×10^6 cells) were seeded in 35-mm dishes and cultured with Dox for 48 h. They were then treated with cycloheximide (CHX) for indicated time periods. Cell lysates were immunoblotted with indicated antibodies (B). The graph (C) shows the densitometric quantification of E-cadherin protein.

Figure S5. Validation of PRL-targeting MOs and phenotypes of MO-injected zebrafish larvae.

(A) Schematic illustration of four mRNA constructs where 5′-UTR and 5′-ORF regions of zebrafish PRL genes (*ptp4a1*, *ptp4a2a*, *ptp4a2b variant 1* and *ptp4a2b variant 2*) are fused with *EGFP*. The targeting site of each MO spanning the translation initiation site is

indicated by the bold black line.

(B) 100 pg of each mRNA construct indicated in (A) was co-injected with 6.8 ng of control MO (upper layer) or respective MO (lower layer). Stereo-microscopic images and EGFP fluorescence images are shown. Scale bar, 1 mm.

(C, D) Zebrafish embryos were injected with control MO (6.8 ng), each of the four MOs (1.7 ng), or PRL MOs (6.8 ng, a mixture of 1.7 ng of each of the four MOs). Stereo-microscopic images of the injected embryos at 24 hpf are shown (C). Scale bar, 350 μm. The graph (D) shows the percentage of zebrafish larvae with shorter anterior-posterior axes at 24 hpf. Each zebrafish larva was visually categorized into one of the three groups as shown in the right panels, based on the severity of the phenotype.

Figure S6. Schematic illustration showing the measurement of electrical resistance across the epithelial sheet.

Cells were seeded on a membrane of transwell insert and cultured for 48 h after Dox. One electrode is placed in the upper chamber and the other in the lower chamber, and electrical resistance across the epithelial sheet was measured (See Materials and Methods for the detailed protocol).

Figure 1

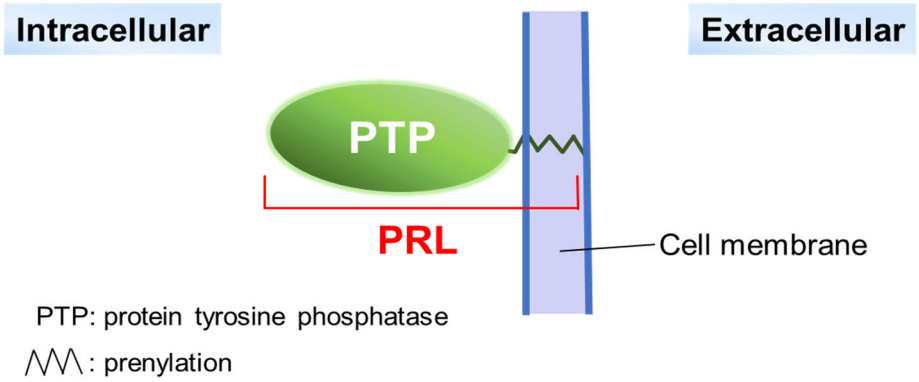
Intracellular
Extracellular
PTP
PRL
Cell membrane
PTP: protein tyrosine phosphatase
: prenylation

Figure 2

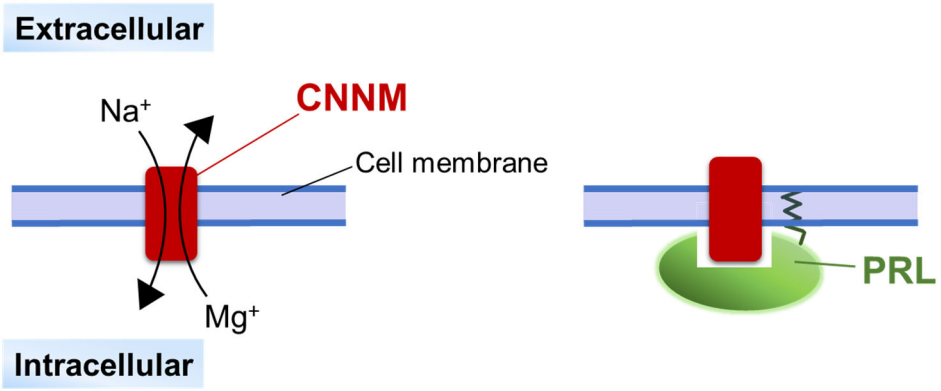

Figure 3

- ***Prl1*-KO or *Prl3*-KO**

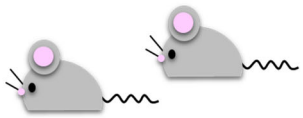

No obvious phenotype

(Bai et al., 2016; Zimmerman et al., 2013)

- ***Prl2*-KO**

Mild phenotype
(growth retardation and reduced fertility)

(Dong et al., 2012; Dong et al., 2014)

- ***Prl1*- and *Prl2*- double KO**

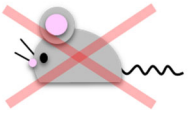

Embryonic lethal

(Bai et al., 2016)

Figure 4

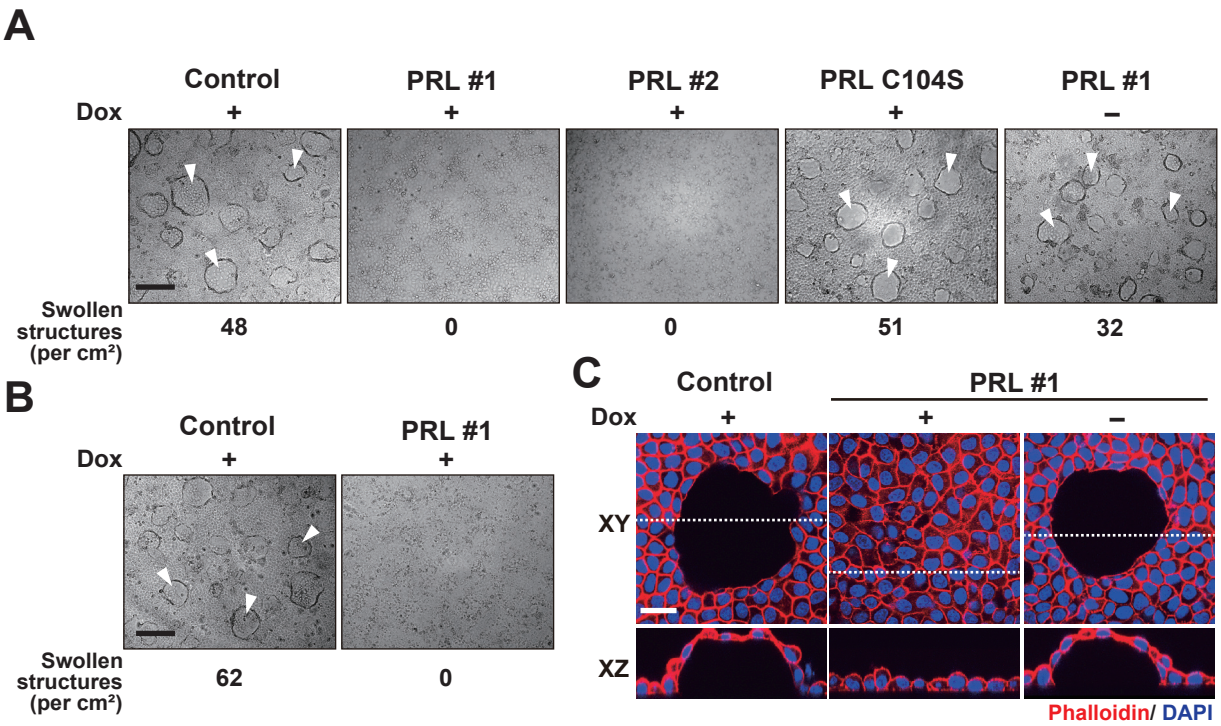
A
Control
PRL #1
PRL #2
PRL C104S
PRL #1
Dox
+
+
+
+
–
Swollen structures (per cm²)
48
0
0
51
32
B
Control
PRL #1
Dox
+
+
Swollen structures (per cm²)
62
0
C
Control
PRL #1
Dox
+
+
–
XY
XZ
Phalloidin/ DAPI

Figure 5

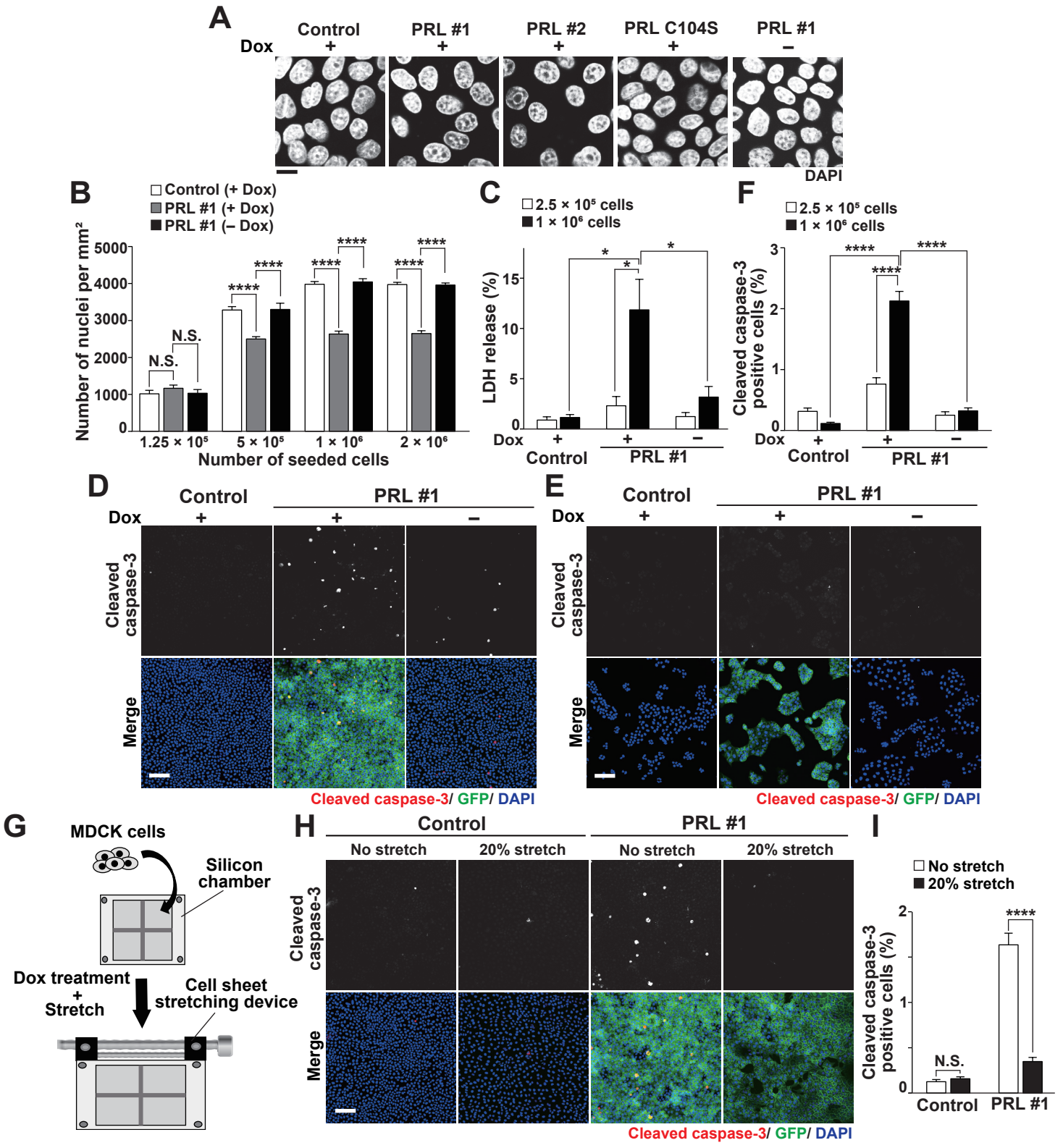
A
Dox
Control
PRL #1
PRL #2
PRL C104S
PRL #1
+
+
+
+
–
DAPI
B
Control (+ Dox)
PRL #1 (+ Dox)
PRL #1 (– Dox)
Number of nuclei per mm²
5000
4000
3000
2000
1000
0
N.S.
N.S.
****
****
****
****
****
1.25 × 10⁵
5 × 10⁵
1 × 10⁶
2 × 10⁶
Number of seeded cells
C
2.5 × 10⁵ cells
1 × 10⁶ cells
LDH release (%)
15
10
5
0
*
*
*
Dox
+
+
–
Control
PRL #1
F
2.5 × 10⁵ cells
1 × 10⁶ cells
Cleaved caspase-3 positive cells (%)
3
2
1
0
****
****
****
Dox
+
+
–
Control
PRL #1
D
Control
PRL #1
Dox
+
+
–
Cleaved caspase-3
Merge
Cleaved caspase-3/ GFP/ DAPI
E
Control
PRL #1
Dox
+
+
–
Cleaved caspase-3
Merge
Cleaved caspase-3/ GFP/ DAPI
G
MDCK cells
Silicon chamber
Dox treatment + Stretch
Cell sheet stretching device
H
Control
PRL #1
No stretch
20% stretch
No stretch
20% stretch
Cleaved caspase-3
Merge
Cleaved caspase-3/ GFP/ DAPI
I
No stretch
20% stretch
Cleaved caspase-3 positive cells (%)
2
1
0
****
N.S.
Control
PRL #1

Figure 6

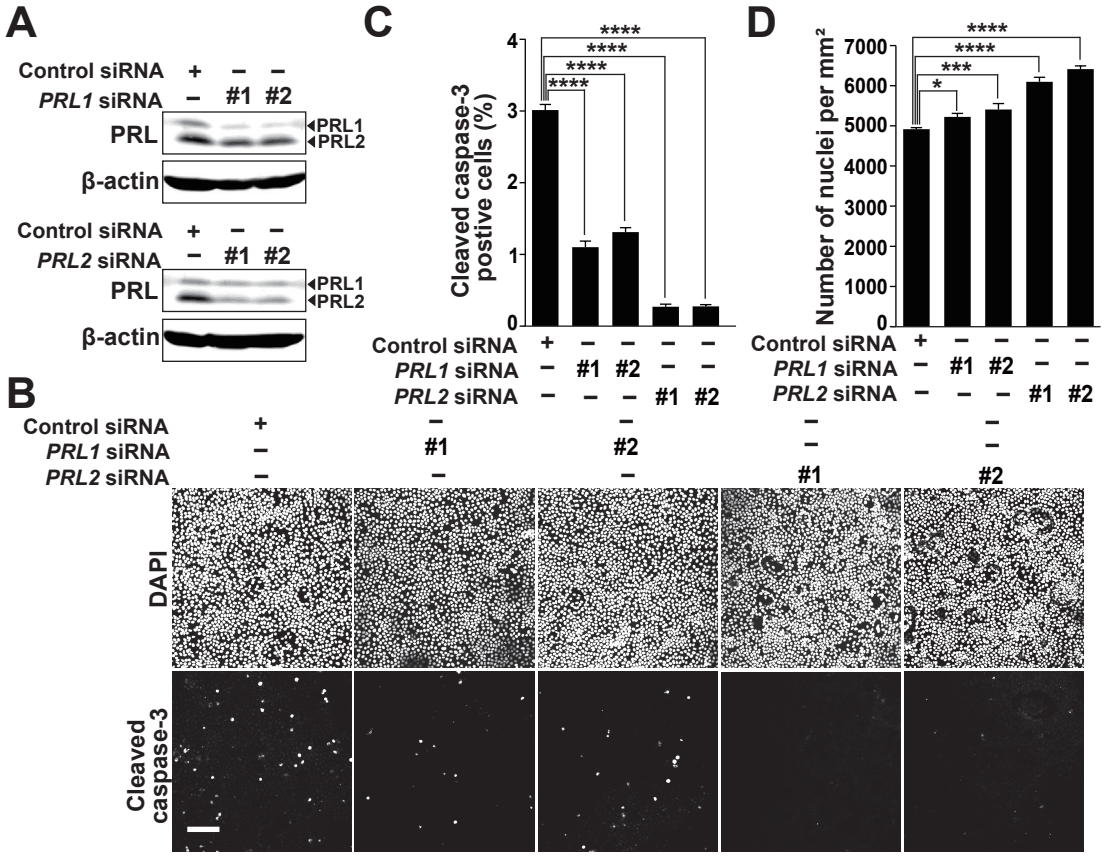
A
Control siRNA + – –
PRL1 siRNA – #1 #2
PRL
PRL1
PRL2
β-actin
Control siRNA + – –
PRL2 siRNA – #1 #2
PRL
PRL1
PRL2
β-actin
B
Control siRNA +
PRL1 siRNA –
PRL2 siRNA –
– – – –
#1 #2 #1 #2
DAPI
Cleaved caspase-3
C
Cleaved caspase-3 postive cells (%)
0 1 2 3 4
****
****
****
****
Control siRNA + – – – –
PRL1 siRNA – #1 #2 – –
PRL2 siRNA – – – #1 #2
D
Number of nuclei per mm²
0 1000 2000 3000 4000 5000 6000 7000
****
****
***
*
Control siRNA + – – – –
PRL1 siRNA – #1 #2 – –
PRL2 siRNA – – – #1 #2

Figure 7

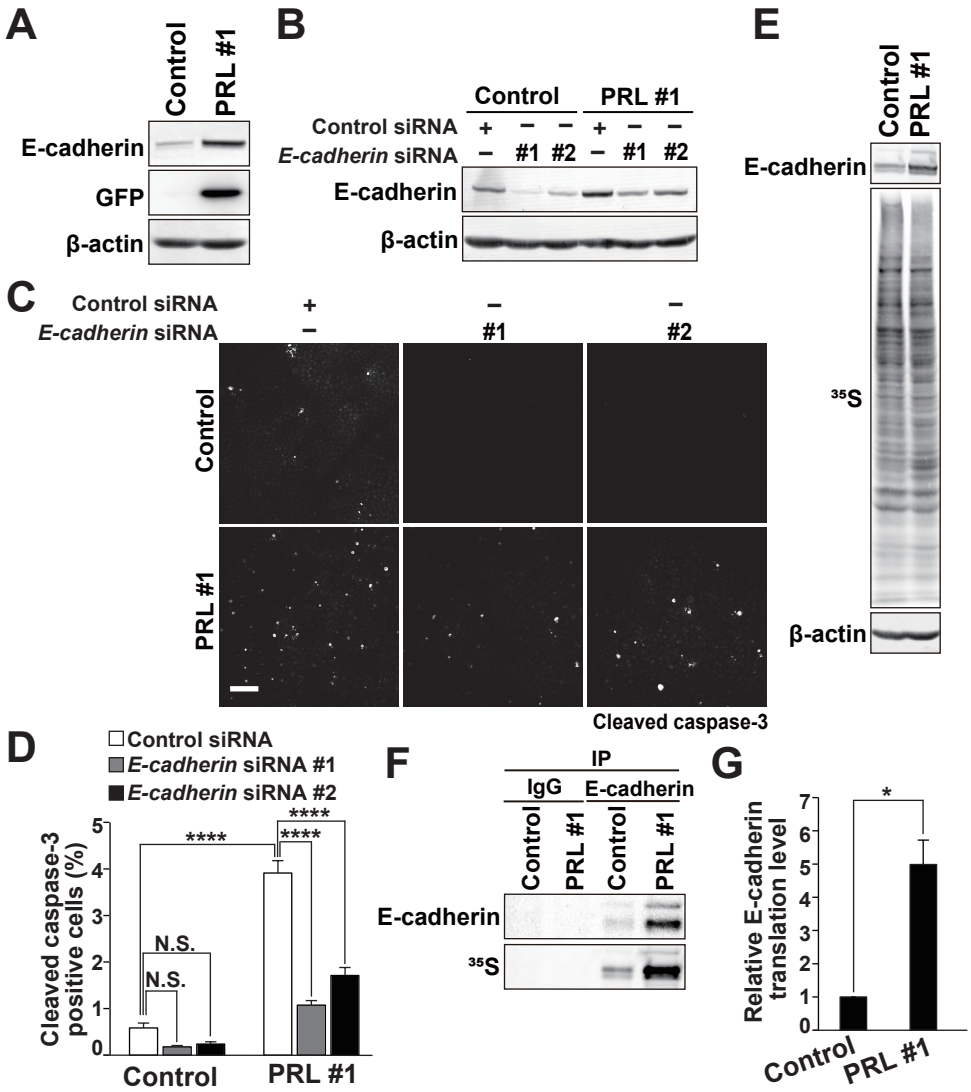
A
Control
PRL #1
E-cadherin
GFP
β-actin
B
Control
PRL #1
Control siRNA + – – + – –
E-cadherin siRNA – #1 #2 – #1 #2
E-cadherin
β-actin
E
Control
PRL #1
E-cadherin
35S
β-actin
C
Control siRNA + – –
E-cadherin siRNA – #1 #2
Control
PRL #1
Cleaved caspase-3
D
Control siRNA
E-cadherin siRNA #1
E-cadherin siRNA #2
Cleaved caspase-3 positive cells (%)
****
****
****
N.S.
N.S.
Control
PRL #1
F
IP
IgG
E-cadherin
Control
PRL #1
Control
PRL #1
E-cadherin
35S
G
Relative E-cadherin translation level
*
Control
PRL #1

Figure 8

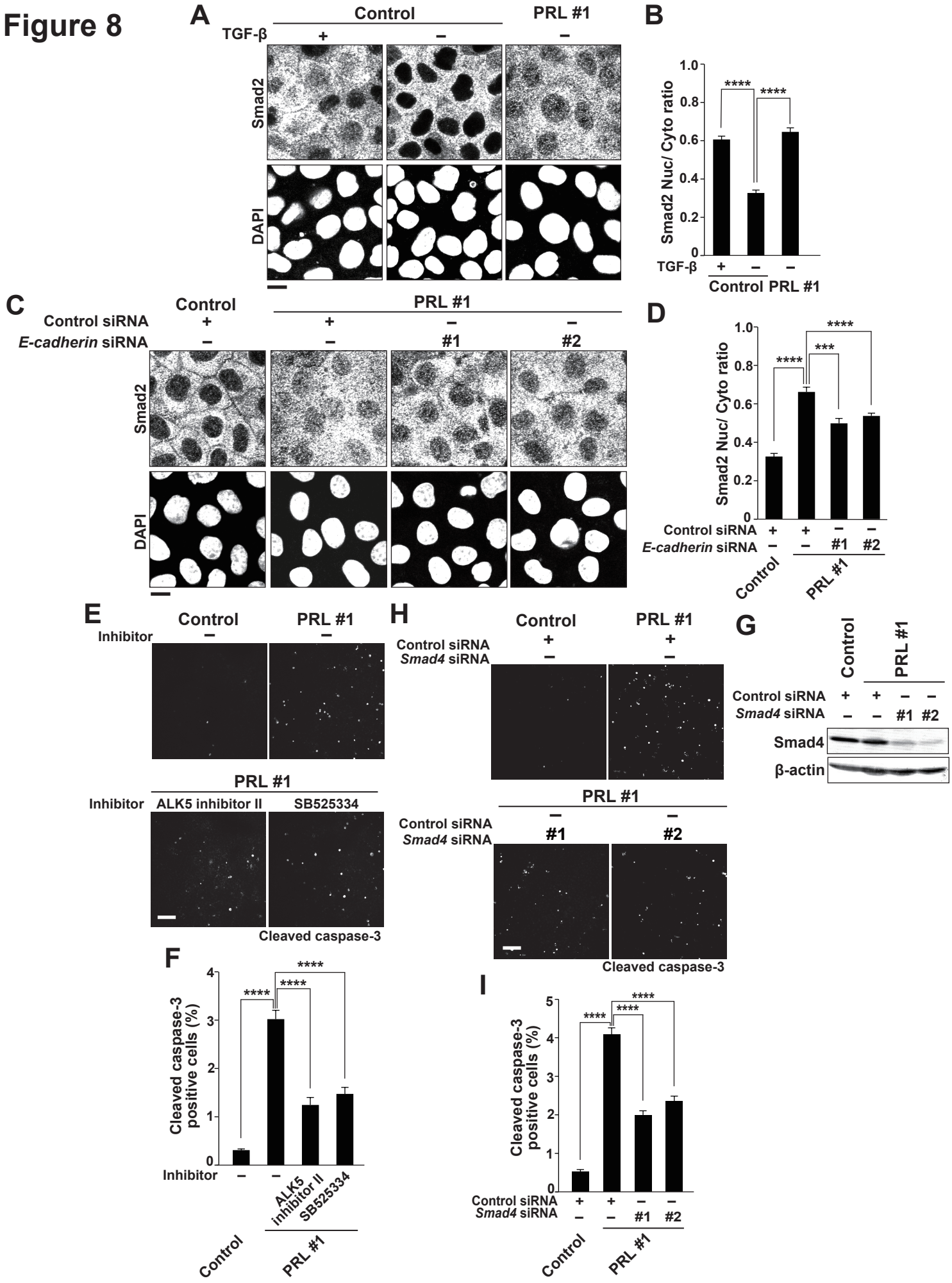
A
Control
PRL #1
TGF-β
+
–
–
Smad2
DAPI
B
Smad2 Nuc/ Cyto ratio
1.0
0.8
0.6
0.4
0.2
0
****
****
TGF-β
+
–
–
Control
PRL #1
C
Control
PRL #1
Control siRNA
+
+
–
–
E-cadherin siRNA
–
–
#1
#2
Smad2
DAPI
D
Smad2 Nuc/ Cyto ratio
1.0
0.8
0.6
0.4
0.2
0
****
***
****
Control siRNA
+
+
–
–
E-cadherin siRNA
–
–
#1
#2
Control
PRL #1
E
Control
PRL #1
Inhibitor
–
–
PRL #1
Inhibitor
ALK5 inhibitor II
SB525334
Cleaved caspase-3
H
Control
PRL #1
Control siRNA
+
+
Smad4 siRNA
–
–
PRL #1
–
–
Control siRNA
#1
#2
Smad4 siRNA
Cleaved caspase-3
G
Control
PRL #1
Control siRNA
+
+
–
–
Smad4 siRNA
–
–
#1
#2
Smad4
β-actin
F
Cleaved caspase-3 positive cells (%)
4
3
2
1
0
****
****
****
Inhibitor
–
–
ALK5 inhibitor II
SB525334
Control
PRL #1
I
Cleaved caspase-3 positive cells (%)
5
4
3
2
1
0
****
****
****
Control siRNA
+
+
–
–
Smad4 siRNA
–
–
#1
#2
Control
PRL #1

Figure 9

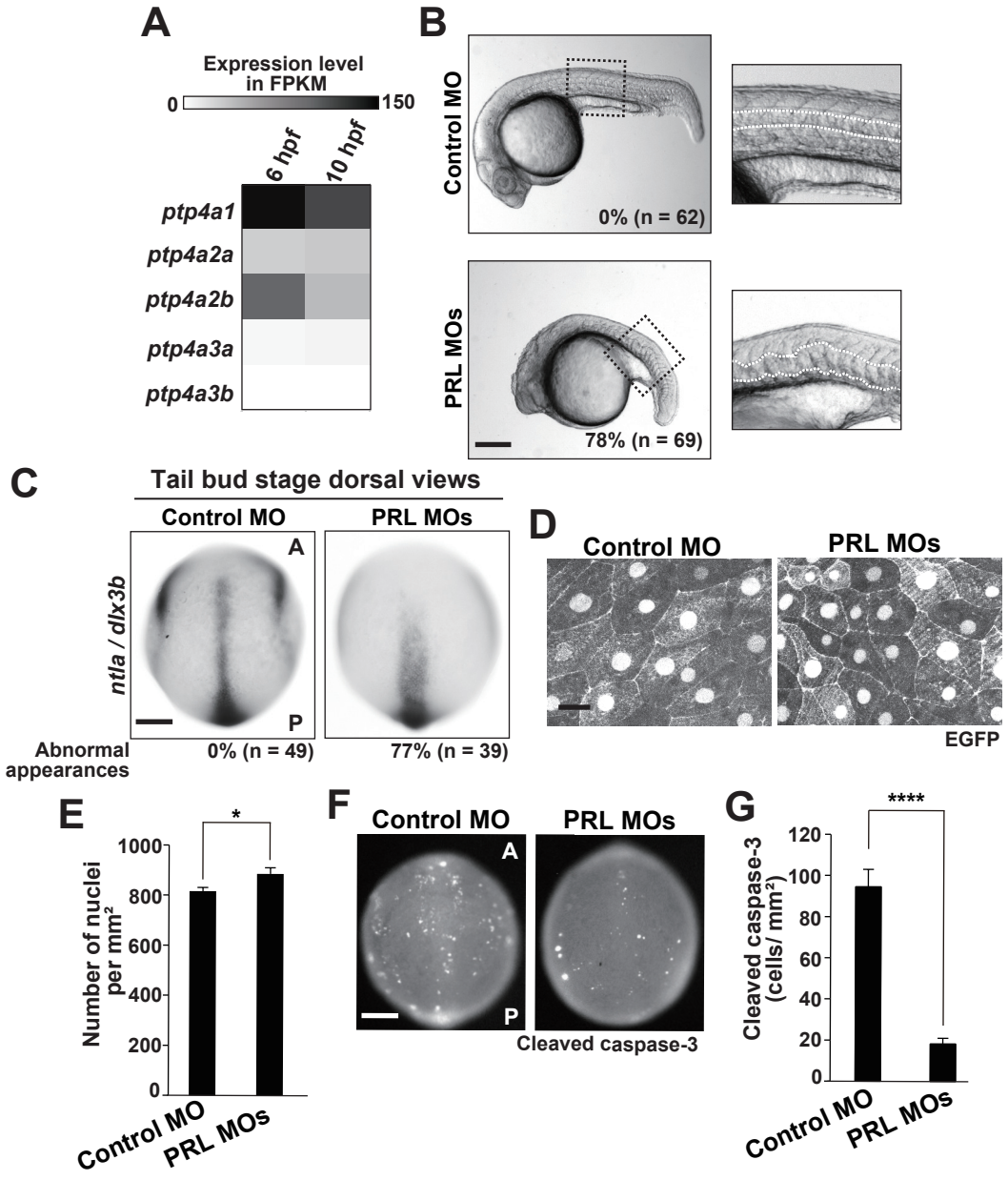
A
Expression level in FPKM
0
150
6 hpf
10 hpf
ptp4a1
ptp4a2a
ptp4a2b
ptp4a3a
ptp4a3b
B
Control MO
0% (n = 62)
PRL MOs
78% (n = 69)
C
Tail bud stage dorsal views
Control MO
PRL MOs
ntla / dlx3b
A
P
Abnormal appearances
0% (n = 49)
77% (n = 39)
D
Control MO
PRL MOs
EGFP
E
Number of nuclei per mm²
1000
800
600
400
200
0
*
Control MO
PRL MOs
F
Control MO
PRL MOs
A
P
Cleaved caspase-3
G
Cleaved caspase-3 (cells/ mm²)
120
100
80
60
40
20
0
****
Control MO
PRL MOs

Figure S1

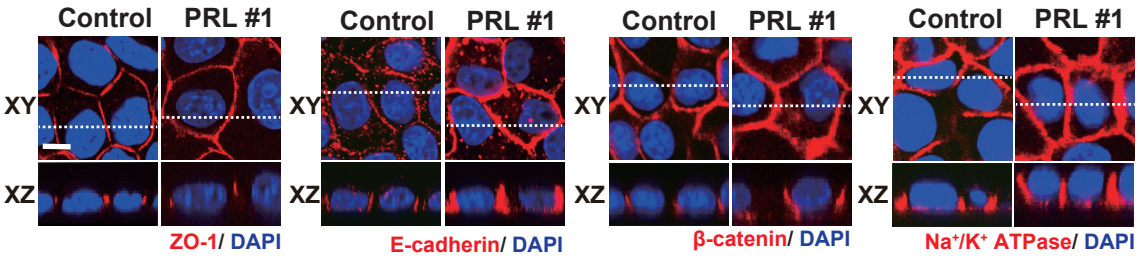
Control
PRL #1
XY
XZ
ZO-1/ DAPI
E-cadherin/ DAPI
β-catenin/ DAPI
Na+/K+ ATPase/ DAPI

Figure S2

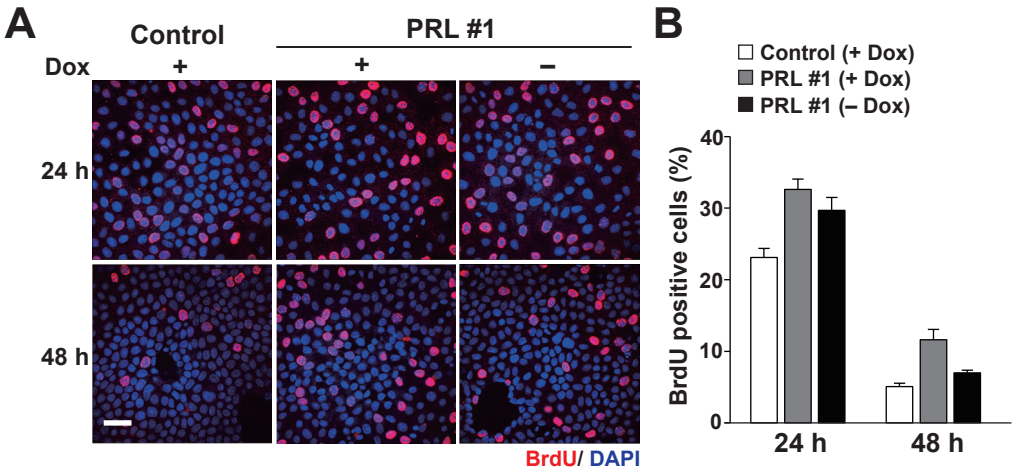
A
Control
PRL #1
Dox
+
+
–
24 h
48 h
BrdU/ DAPI
B
Control (+ Dox)
PRL #1 (+ Dox)
PRL #1 (– Dox)
BrdU positive cells (%)
40
30
20
10
0
24 h
48 h

Figure S3

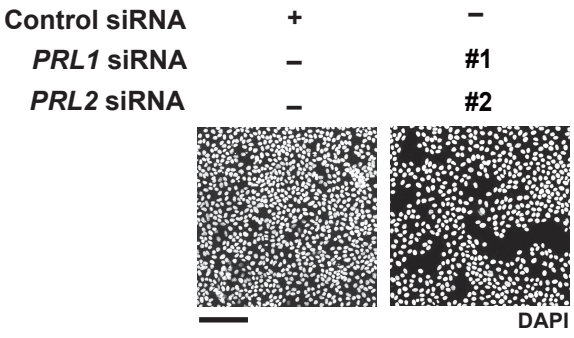

Figure S4

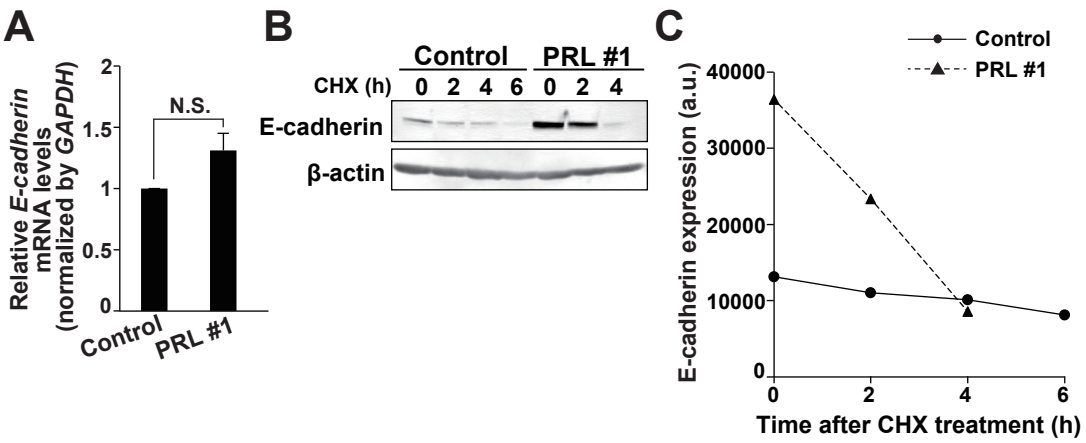
A
Relative E-cadherin mRNA levels (normalized by GAPDH)
2
1.5
1
0.5
0
N.S.
Control
PRL #1
B
Control
PRL #1
CHX (h)
0 2 4 6 0 2 4
E-cadherin
β-actin
C
Control
PRL #1
E-cadherin expression (a.u.)
40000
30000
20000
10000
0
0 2 4 6
Time after CHX treatment (h)

Figure S5

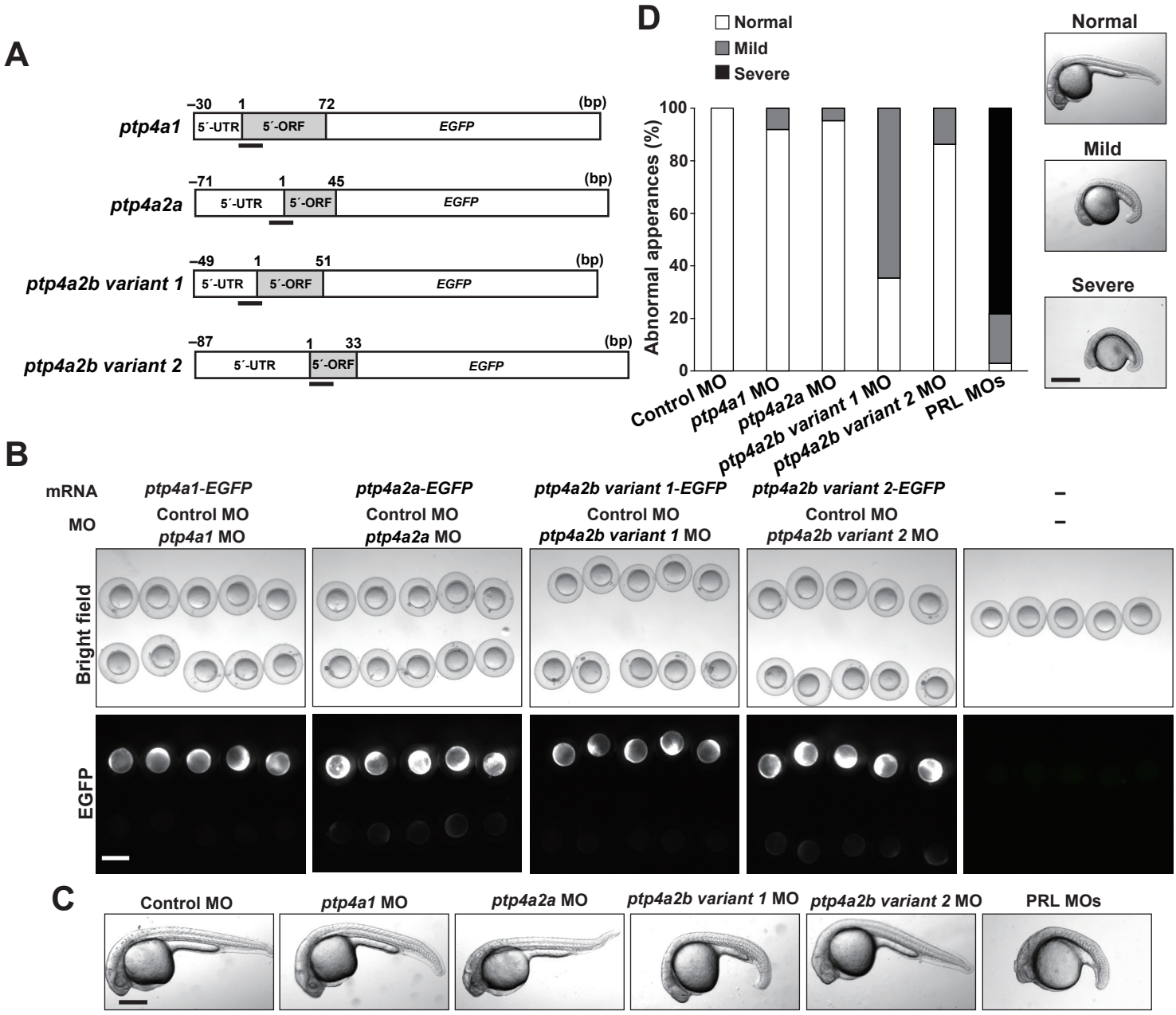
A
ptp4a1
−30 1 72 (bp)
5′-UTR
5′-ORF
EGFP
ptp4a2a
−71 1 45 (bp)
ptp4a2b variant 1
−49 1 51 (bp)
ptp4a2b variant 2
−87 1 33 (bp)
D
Normal
Mild
Severe
Abnormal apperances (%)
100
80
60
40
20
0
Control MO
ptp4a1 MO
ptp4a2a MO
ptp4a2b variant 1 MO
ptp4a2b variant 2 MO
PRL MOs
Normal
Mild
Severe
B
mRNA
MO
ptp4a1-EGFP
Control MO
ptp4a1 MO
ptp4a2a-EGFP
Control MO
ptp4a2a MO
ptp4a2b variant 1-EGFP
Control MO
ptp4a2b variant 1 MO
ptp4a2b variant 2-EGFP
Control MO
ptp4a2b variant 2 MO
Bright field
EGFP
C
Control MO
ptp4a1 MO
ptp4a2a MO
ptp4a2b variant 1 MO
ptp4a2b variant 2 MO
PRL MOs

Figure S6

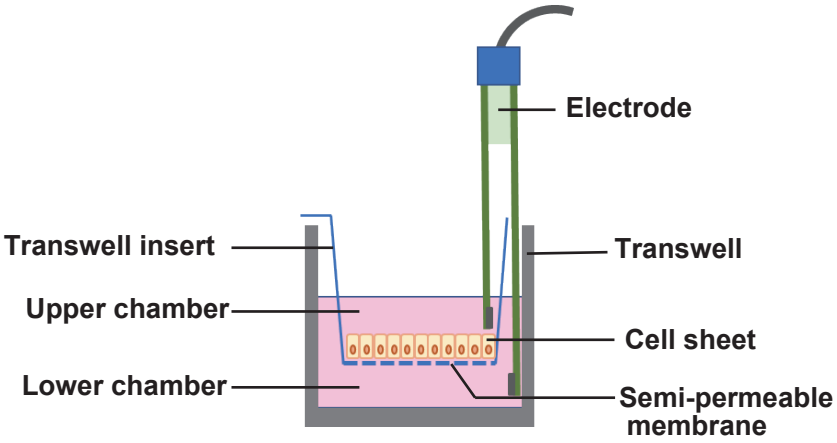
Electrode
Transwell insert
Transwell
Upper chamber
Cell sheet
Lower chamber
Semi-permeable membrane

Appendices

Appendix 1

PRL3 was overexpressed in zebrafish embryos by injecting mouse *Prl3*-mRNA. For the mRNA microinjection, template plasmids were constructed. Briefly, flag-tagged full length wild-type mouse Prl3 fragment from pEF-BOS-flag-Prl3 plasmid (Ishii et al., 2013) were inserted into XbaI site of pCS2 vector to construct pCS2-flag-Prl3. The plasmid constructs were then linearized, and transcribed *in vitro* using mMESSAGE mMACHINE™ SP6 Transcription Kit (ThermoFisher Scientific, AM1340) according to the manufacturer's instructions. Proper synthesis of each mRNA was verified by agarose gel electrophoresis. After microinjecting 800 pg of synthesized mRNA, phenotypes were compared with non-injected wild-type larva.

The preliminary result showed different phenotypes upon overexpression of Prl3 at 32 hpf. For instance, fusion of eyes, loss of pigmentation, non-motile or presence of convulsion after touching the body of larva (Appendix 1A and 1B).

Appendix 2

When each of the MO was injected into one-cell stage zebrafish embryos, phenotypes such as mild curvature of back, loss of motility, loss of pigmentation were observed at 36 hpf (Appendix 2A and 2B). In addition, for those injected with mixture of all four MOs (PRL MOs), phenotypes such as loss of pigmentation and loss of motility were observed at 48 hpf (Appendix 2C and 2D).

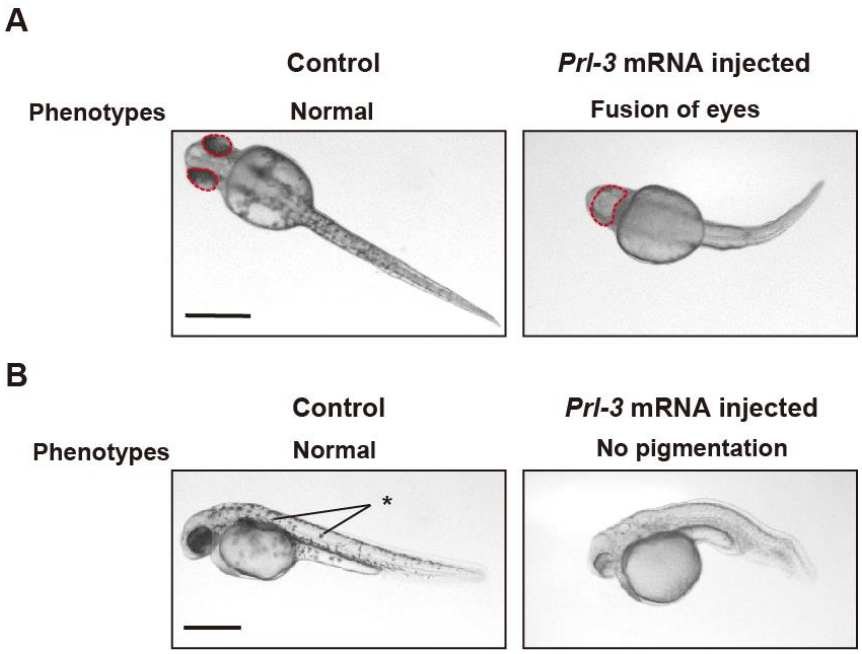

Appendix 1. Phenotypes of mouse *Prl-3* mRNA-injected zebrafish larvae at 32 hpf.

(A , B) 800 pg of mouse *Prl-3* mRNA was injected and phenotypes of zebrafish larvae was compared with wild-type larvae (control). Stereo-microscopic images taken at 32 hpf are shown. Ventral view of larvae where the red dotted lines outline the border of eyes (A). Lateral view of larvae showing pigmentation (*, black spots) on the body surface (B). Scale bar, 500 μm.

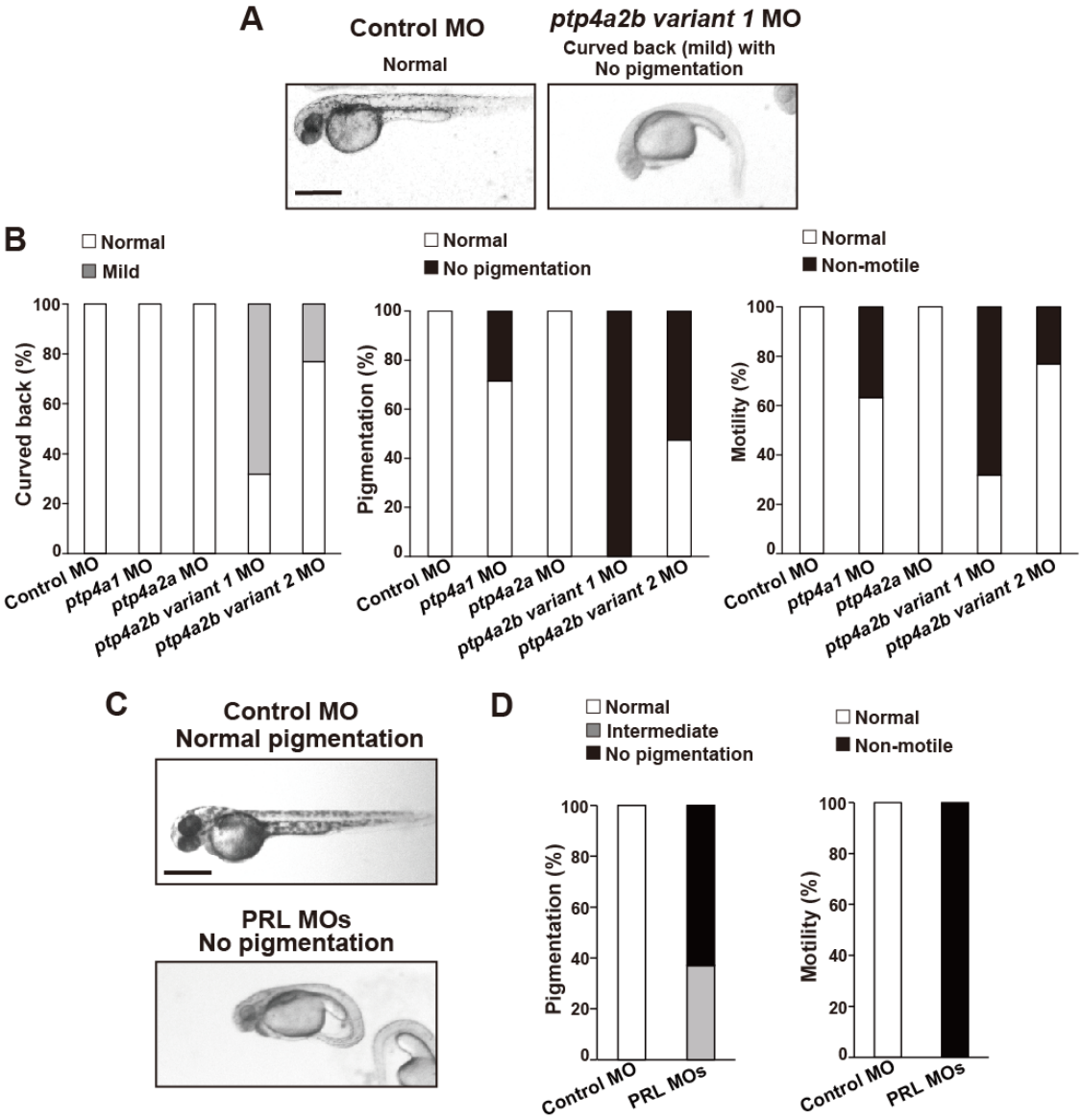

Appendix 2. Phenotypes of MO-injected zebrafish larvae after 24 hpf.

(A-D) Zebrafish embryos were injected with control MO (6.8 ng), each of the four MOs (1.7 ng for A and B), or PRL MOs (6.8 ng, a mixture of 1.7 ng of each of the four MOs, for C and D). Stereo-microscopic images of MO-injected larvae at 36 hpf (A) and 48 hpf (C) are shown. Scale bar, 500 μm. Graphs show the percentage of larvae with curved back (left, n = 17 to 50), the percentage of larvae having pigmentation on the body surface (middle, n = 14 to 50), and the percentage of larvae showing motility after touching (right, n = 16 to 50) (B). Phenotypes of each zebrafish larva in graph (B) was classified as in (A). Graphs shows the percentage of larvae with pigmentation (left, n = 27 to 43) and those showing motility after touching (right, n = 27 to 43) (D). The percentage of larvae having no pigmentation in graph (D) was classified as in (C), and the one with moderate pigmentation pattern were classified as intermediate.

Appendices reference

Ishii, T., Funato, Y., and Miki, H. (2013). Thioredoxin-related protein 32 (TRP32) specifically reduces oxidized phosphatase of regenerating liver (PRL). J Biol Chem. *288*, 7263–7270.

Achievements

Publication

A novel role of PRL in regulating epithelial cell density by inducing apoptosis at confluence

Sweksha Lohani, Yosuke Funato, Yuki Akieda, Tohru Ishitani, Hiroaki Miki. (Submitted)

Presentations

1. A novel role of PRL in regulating epithelial cell density by inducing apoptosis at confluence

   2020 Research Institute for Microbial Diseases (RIMD) Annual Research Meeting, Online, 22nd January, 2021 (Oral presentation and Poster presentation)

   Sweksha Lohani

2. PRL determines epithelial cell density by inducing apoptosis at confluence

   43rd Annual meeting of the Molecular Biology Society of Japan, Online, 4th December, 2020 (Poster presentation)

   Sweksha Lohani, Yosuke Funato, Hiroaki Miki

3. PRL determines epithelial cell density by inducing apoptosis at confluence

   11th Interdisciplinary Program for Biomedical Sciences (IPBS) Progress Report

Meeting, The Leading Graduate School, Osaka University, 26th November, 2020 (Poster presentation)

Sweksha Lohani, Yosuke Funato, Hiroaki Miki

4. PRL-3 drives density-dependent death of MDCK cells

   10th IPBS Progress Report Meeting, The Leading Graduate School, Osaka University, 16th December, 2019 (Poster presentation)

   Sweksha Lohani, Yosuke Funato, Hiroaki Miki

5. PRL drives density-dependent death of MDCK cells

   92nd Annual meeting of the Japanese biochemical society, Yokohama, 18th September, 2019 (Oral presentation and Poster presentation)

   Sweksha Lohani, Yosuke Funato, Hiroaki Miki

6. The role of phosphatase of regenerating liver-3 (PRL-3) in epithelial homeostasis

   9th IPBS Progress Report Meeting, The Leading Graduate School, Osaka University, 23rd January, 2018 (Poster presentation)

   Sweksha Lohani, Yosuke Funato, Hiroaki Miki

Awards

1. RIMD Annual Research Meeting (2021), Excellent Academic Award
2. 11th IPBS Progress Report Meeting (2020), Best Poster Award
3. 10th IPBS Progress Report Meeting (2019), Best Poster Award

Grant achievement

1. The Leading Graduate School Program: IPBS Grant-in-Aid for Interdisciplinary Research 2020.